NASA/CR—2012-217665

Radioisotope Stirling Engine Powered Airship for Low Altitude Operation on Venus

Anthony J. Colozza
Qinetiq North America, Cleveland, Ohio

August 2012

NASA STI Program . . . in Profile

Since its founding, NASA has been dedicated to the advancement of aeronautics and space science. The NASA Scientific and Technical Information (STI) program plays a key part in helping NASA maintain this important role.

The NASA STI Program operates under the auspices of the Agency Chief Information Officer. It collects, organizes, provides for archiving, and disseminates NASA's STI. The NASA STI program provides access to the NASA Aeronautics and Space Database and its public interface, the NASA Technical Reports Server, thus providing one of the largest collections of aeronautical and space science STI in the world. Results are published in both non-NASA channels and by NASA in the NASA STI Report Series, which includes the following report types:

- TECHNICAL PUBLICATION. Reports of completed research or a major significant phase of research that present the results of NASA programs and include extensive data or theoretical analysis. Includes compilations of significant scientific and technical data and information deemed to be of continuing reference value. NASA counterpart of peer-reviewed formal professional papers but has less stringent limitations on manuscript length and extent of graphic presentations.

- TECHNICAL MEMORANDUM. Scientific and technical findings that are preliminary or of specialized interest, e.g., quick release reports, working papers, and bibliographies that contain minimal annotation. Does not contain extensive analysis.

- CONTRACTOR REPORT. Scientific and technical findings by NASA-sponsored contractors and grantees.

- CONFERENCE PUBLICATION. Collected papers from scientific and technical conferences, symposia, seminars, or other meetings sponsored or cosponsored by NASA.

- SPECIAL PUBLICATION. Scientific, technical, or historical information from NASA programs, projects, and missions, often concerned with subjects having substantial public interest.

- TECHNICAL TRANSLATION. English-language translations of foreign scientific and technical material pertinent to NASA's mission.

Specialized services also include creating custom thesauri, building customized databases, organizing and publishing research results.

For more information about the NASA STI program, see the following:

- Access the NASA STI program home page at *http://www.sti.nasa.gov*

- E-mail your question to *help@sti.nasa.gov*

- Fax your question to the NASA STI Information Desk at 443–757–5803

- Phone the NASA STI Information Desk at 443–757–5802

- Write to:
  STI Information Desk
  NASA Center for AeroSpace Information
  7115 Standard Drive
  Hanover, MD 21076–1320

NASA/CR—2012-217665

Radioisotope Stirling Engine Powered Airship for Low Altitude Operation on Venus

Anthony J. Colozza
Qinetiq North America, Cleveland, Ohio

Prepared under Contract NNC07E252T-8

National Aeronautics and
Space Administration

Glenn Research Center
Cleveland, Ohio 44135

August 2012

Level of Review: This material has been technically reviewed by NASA technical management OR expert reviewer(s).

Available from

NASA Center for Aerospace Information
7115 Standard Drive
Hanover, MD 21076–1320

National Technical Information Service
5301 Shawnee Road
Alexandria, VA 22312

Available electronically at http://www.sti.nasa.gov

Contents

Radioisotope Stirling Engine Powered Airship for Low Altitude Operation on Venus

Anthony J. Colozza
Qinetiq North America
Cleveland, Ohio 44135

Abstract

The feasibility of a Stirling engine powered airship for the near surface exploration of Venus was evaluated. The heat source for the Stirling engine was limited to 10 general purpose heat source (GPHS) blocks. The baseline airship utilized hydrogen as the lifting gas and the electronics and payload were enclosed in a cooled insulated pressure vessel to maintain the internal temperature at 320 K and 1 Bar pressure. The propulsion system consisted of an electric motor driving a propeller. An analysis was set up to size the airship that could operate near the Venus surface based on the available thermal power. The atmospheric conditions on Venus were modeled and used in the analysis. The analysis was an iterative process between sizing the airship to carry a specified payload and the power required to operate the electronics, payload and cooling system as well as provide power to the propulsion system to overcome the drag on the airship. A baseline configuration was determined that could meet the power requirements and operate near the Venus surface. From this baseline design additional trades were made to see how other factors affected the design such as the internal temperature of the payload chamber and the flight altitude. In addition other lifting methods were evaluated such as an evacuated chamber, heated atmospheric gas and augmented heated lifting gas. However none of these methods proved viable.

1.0 Introduction

Venus, shown in Figure 1.1, is the second planet from the Sun and is similar to Earth in size and density, but that is where the similarities end. Its atmospheric pressure near the surface is 90 times that of Earth's and the surface temperature is around 455 °C. The high surface temperature and pressure pose an inhospitable environment for materials, mechanisms and electronics. Because of this the exploration of the surface and lower atmosphere of Venus has been fairly limited. The Russian Venera series of landers are the only probes to successfully send data back to Earth from the Venus surface, as shown in Figure 1.1. These landers, however only survived for a short period of time, from approximately 20 minutes to a few hours, on the surface. To return the maximum amount of scientific data a vehicle that can survive for extended periods of time and is mobile enabling it to move about the surface or atmosphere in a controlled manner would be ideal. By being able to explore different surface features and locations, similar to the Mars rovers (Spirit and Opportunity) this type of vehicle can provide significant insight into the geology and surface/atmospheric conditions of Venus.

Venus however is much different than Mars and an exploration vehicle designed for operation on Venus will have significantly different characteristics and requirements than one utilized on Mars. The first difference is related to the power source for the vehicle. On Mars photovoltaic arrays can be utilized as a power source, whereas on Venus, even though it is closer to the Sun, the thick cloud cover encompassing the planet, as well as the high surface temperature, makes utilizing solar power difficult. Therefore a different power source is required, one based on the conversion of heat generated through radioactive decay of Plutonium to electricity. These radioisotope heat sources are commonly utilized for deep space missions, where insufficient solar energy is available, and similarly can be utilized for a Venus surface mission. The one downside to a radioisotope based power system is that they tend to be heavier than an equivalent PV based system. This is critical since for a mobile vehicle the lower its mass the less power will be required to move. Therefore, maximizing the thermal to electrical conversion efficiency is a critical factor in the power system design. Of the available thermal to electrical conversion systems, a Stirling engine provides the highest efficiency and therefore the greatest benefit to the vehicle.

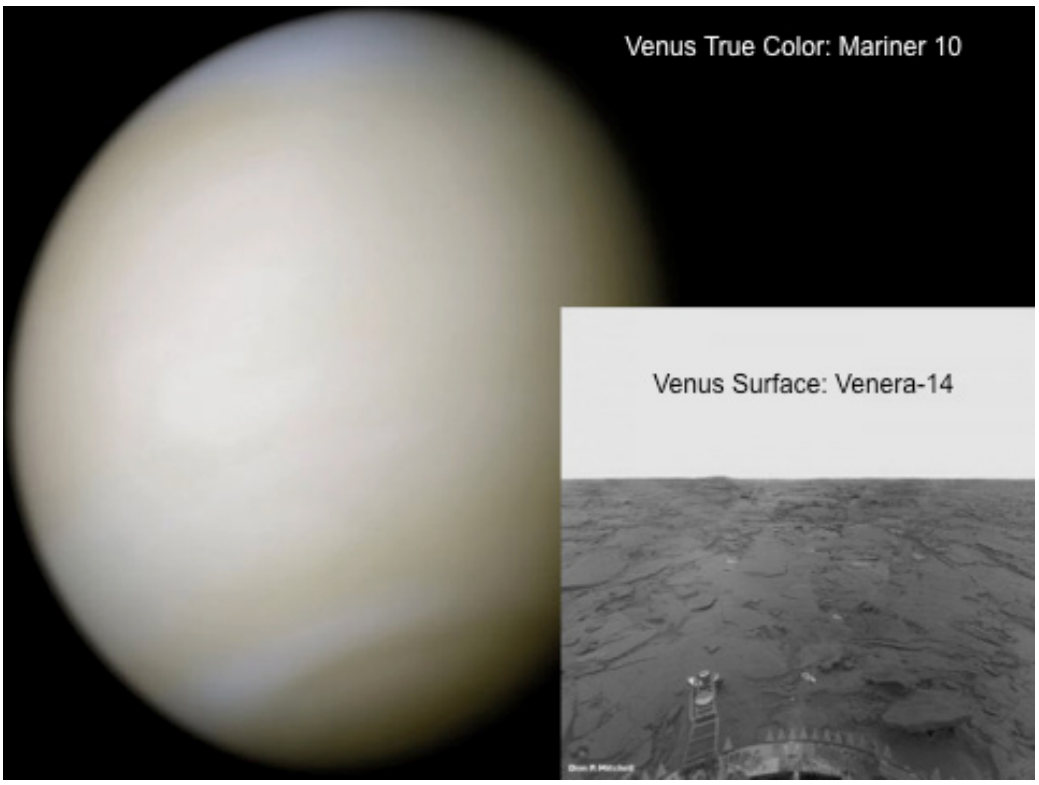

Figure 1.1.—True color image of Venus from Mariner 10 (Ref. 1) and surface image from the Soviet Venera-14 (Ref. 2).

The difference between the atmosphere of Venus and Mars also factor into the type of vehicle which can be used for exploration. Both planet's atmospheres are comprised mainly of CO_2. However, as mentioned previously, Venus's atmosphere is thick and dense whereas the atmosphere of Mars is rarified, with a density near the surface similar to that of Earth's atmosphere at 30 km altitude. The thick, dense atmosphere of Venus provides both benefits and obstacles in the design of a surface vehicle. One advantage is that the high surface density enables the possibility of utilizing a low speed fight vehicle such as an airship. Whereas on Mars this option is not feasible (Ref. 3). An airship provides a number of benefits to scientific exploration. The main advantages include:

- The ability to cover large amounts of surface terrain.
- To capability to descend to the surface and perform scientific investigation at various locations.
- The ability to go over or around obstacles and explore terrain features that would not be accessible to surface vehicles.
- The ability to sample the atmosphere over a range of altitudes.

Although the high surface density is an advantage for an airship in generating lift, the pressure and temperature poses problems for operating equipment and electronics. Because of this the electronics and payload must be contained in a cooled pressure vessel in order to survive for an extended period of time on the surface. The need for a pressure vessel and cooling system adds significant mass and power requirements to any vehicle design.

Overall an airship could provide a unique capability for exploring the surface of Venus. Although technically challenging, as the design and development of any surface vehicle would be, the airship platform could provide significant terrain coverage as well as the means to explore and sample both the surface and lower atmosphere. This capability would provide unequaled science data return and therefore

should be thoroughly examined as an option for Venus exploration. The analysis and results discussed in this report are a first step in evaluating the feasibility and capabilities of the Stirling engine powered Venus airship concept.

2.0 Atmospheric Environment of Venus

The environmental conditions on Venus are very unique and unlike those on any other known planet or moon. Venus is a place of environmental extremes. Near the surface, the atmospheric temperature is very hot (over 700°K) and the sunlight is dim due to the extensive cloud cover that shrouds the whole planet. The cloud cover extends from approximately 45 km above the surface to approximately 64 km above the surface. At the top of the cloud layer, the atmospheric pressure is around 0.1 bar. Within this altitude range, the atmospheric temperatures are between 80 to –35 °C respectively. The top of the cloud layer corresponds to a pressure altitude of 16 km (52,500 ft) on Earth. A diagram of the Venus atmosphere is shown in Figure 2.1 and the physical and orbital properties of the Venus are shown in Table 2.1.

Another unique aspect of Venus is that the day length is longer than the year. Due to this slow rotational rate, the speed to remain at the same solar time is very low, approximately 13.4 km/hr. This slow rotation rate will enable the airship to operate in daylight for an extended period of time (~120 Earth days).

Because of the thick atmosphere, the pressure and density throughout most of the atmosphere is much greater than that on Earth. The atmospheric pressure and density we experience near the surface of Earth occurs at an altitude of just over 50 km on Venus.

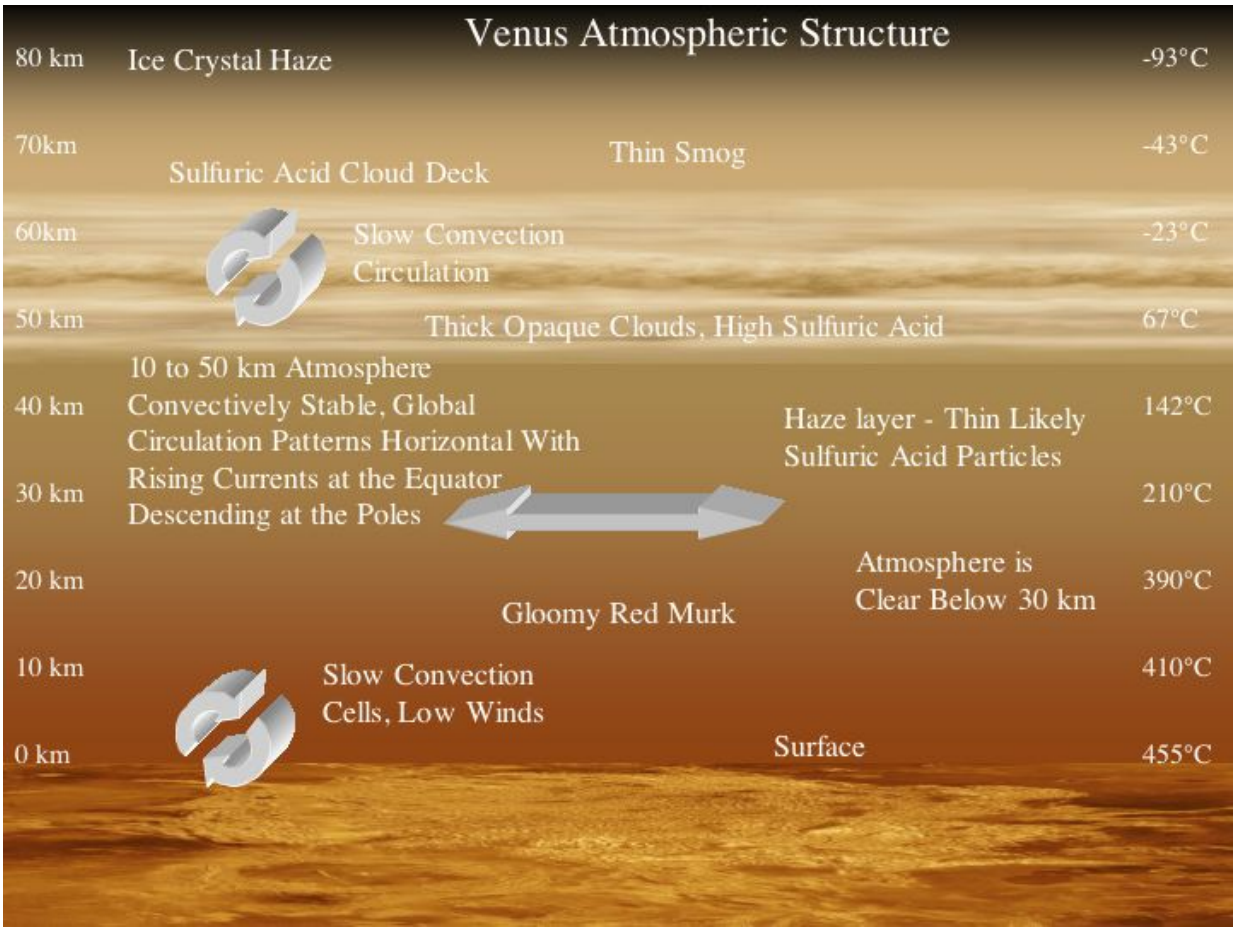

Figure 2.1.—Venus atmospheric structure.

TABLE 2.1.—PHYSICAL AND ORBITAL PROPERTIES OF VENUS (REFS. 1 AND 4)

Property	Value
Maximum Inclination of Equator to Orbit (δ_{max})	3.39°
Orbital Eccentricity (ε)	0.0068
Mean Radius of Orbit (r_m)	108×10^6
Day Period	243 (Earth Days)
Solar Radiation Intensity	Mean: 2613.9 W/m^2
	Parihelion: 2649 W/m^2
	Apehelion: 2579 W/m^2
Albedo	0.67
Gravitational Constant (g_v)	8.87 m/s^2
Sidereal Year	224 (Earth Days)
Surface Temperature	737 °K
Diameter	12,104 km

Above the cloud layer there is an abundant amount of solar energy. The solar flux at the orbit of Venus is 2600 W/m^2, which is much greater than the 1360 W/m^2 available at Earth orbit. At the bottom of the cloud layer (45 km altitude), the solar intensity is between 520 W/m^2 and 1300 W/m^2 depending on the wavelength of the radiation being collected. This is comparable to the solar intensity at Mars or Earth, respectively.

The winds within the atmosphere blow fairly consistently in the same direction as the planetary rotation (East to West) over all latitudes and altitudes up to 100 km. Above 100 km, the winds shift to blow from the dayside of the planet to the night side. The wind speeds decrease as a function of altitude from ~100 m/s at the cloud tops (60 km) to ~0.5 m/s at the surface. These high wind speeds and the slow rotation of the planet produce a super rotation of the atmosphere (nearly 60 times faster than the surface).

The gravitational acceleration on Venus (8.87 m/s^2) is slightly less than that on Earth. The atmospheric composition on Venus is mostly CO_2 but there are also trace amounts of corrosive compounds such as hydrochloric, hydrofluoric and sulfuric acids (Refs. 1 and 4). The atmospheric composition is given in Table 2.2. Because of this composition, the speed of sound within the atmosphere is generally less than it is within Earth's atmosphere.

TABLE 2.2.—VENUS ATMOSPHERIC COMPOSITION (REFS. 1 AND 4)

Gas	Percent volume
Carbon Dioxide (CO_2)	96.5
Nitrogen (N_2)	3.5
Sulfur Dioxide (SO_2)	150 ppm
Carbon Monoxide (CO)	17 ppm
Water Vapor (H_2O)	20 ppm
Neon (Ne)	7 ppm
Argon (Ar)	70 ppm
Helium (He)	17 ppm

The main characteristics of the atmosphere (density, temperature, viscosity, and wind velocity) are critical in determining the feasibility of flight within the Venus atmosphere. These quantities are provided as functions of altitude (z) in kilometers by Equations (2.1) through (2.7) (Ref. 5).

The temperature on Venus (T_a) decreases fairly linearly from the surface up to approximately 60 km in altitude, as seen in Figure 2.2. The temperature as a function of altitude is approximated by Equations (2.1).

$$T_a = 738.26 - 9.1909z + 0.17429z^2 - 0.007965z^3 + 0.0001518z^4 - 1.2336\times10^{-6}z^5 + 3.7325\times10^{-9}z^6 \quad (2.1)$$

Because of the thick atmosphere, the pressure and density throughout most of the atmosphere is much greater than that on Earth. The atmospheric pressure and density we experience near the surface of Earth

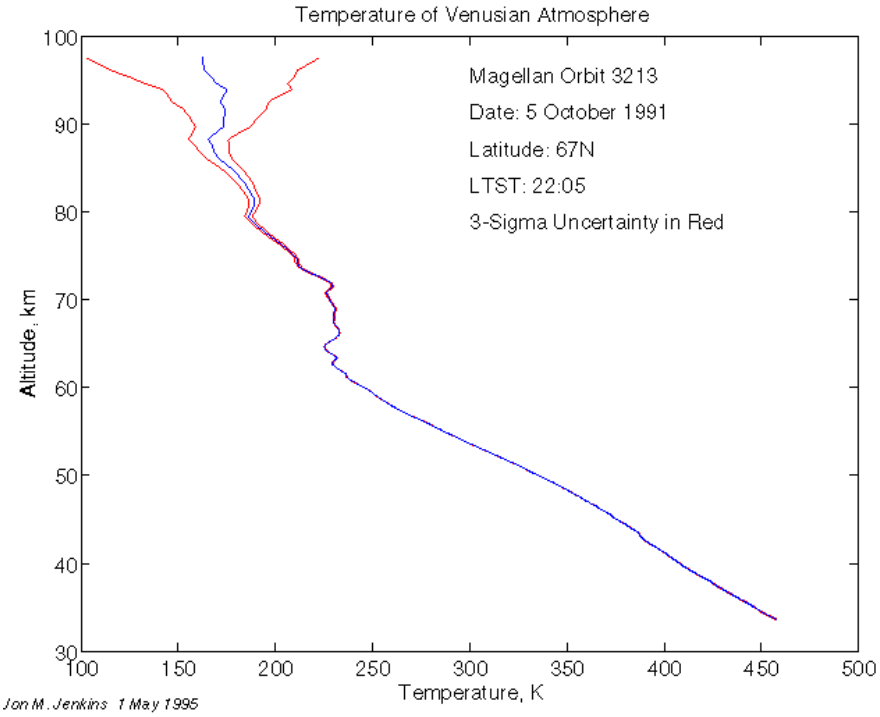

Figure 2.2.—Temperature profile of Venus's atmosphere (Ref. 6).

occurs at an altitude of just over 50 km on Venus. For a flight vehicle, this means that flying at 50 km on Venus is similar aerodynamically to flying near the surface on Earth. The atmospheric density (ρ_a) within the Venus atmosphere can be represented by Equation (2.2) as a function of altitude in kilometers and the viscosity (μ_a) is given by Equation (2.3). This density as a function of altitude is plotted in Figure 2.3.

$$\rho_a = 64.85 - 3.3257z + 0.067373z^2 - 0.00066981z^3 + 3.224\times10^{-6}z^4 - 5.6694\times10^{-9}z^5 - 1.8971\times10^{-12}z^6 \tag{2.2}$$

$$\mu_a = 3.5827\times10^{-5} - 5.906\times10^{-9}z + 8.8642\times10^{-7}z^2 - 5.9485\times10^{-8}z^3 + 2.1929\times10^{-9}z^4 - 4.8611\times10^{-11}z^5 + 6.6513\times10^{-13}z^6 - 5.5001\times10^{-15}z^6 + 2.5199\times10^{-17}z^7 - 4.9099\times10^{-20}z^9 \tag{2.3}$$

The average wind speed on Venus varies considerably from the surface to upper part of the atmosphere. The wind speed near the surface is very low and increases to a maximum of just under 100 m/s at approximately 65 km altitude, as shown in Figure 2.4. A curve fit of mean wind speed (v_a) in meters per second versus altitude in kilometers is given by Equations (2.4) through (2.6). Each of these equations represents a different region of the atmosphere.

Mean wind speed from the surface to 58 km altitude:

$$v_a = 0.89941 - 0.11201z - 0.017082z^2 + 0.0040604z^3 + 0.0010345z^4 - 9.96\times10^{-5}z^5 + 3.28\times10^{-6}z^6 - 4.7\times10^{-8}z^7 + 2.495\times10^{-10}z^8 \tag{2.4}$$

Mean wind speed from 58 to 66 km altitude:

$$v_a = 21498 - 1087.9z + 18.31z^2 - 0.10214z^3 \tag{2.5}$$

Mean wind speed from 66 to 100 km altitude:

$$v_a = -3860.1 + 637.42z - 32.206z^2 + 0.76199z^3 - 0.009357z^4 + 5.783\times10^{-5}z^5 - 1.42\times10^{-7}z^6 \qquad (2.6)$$

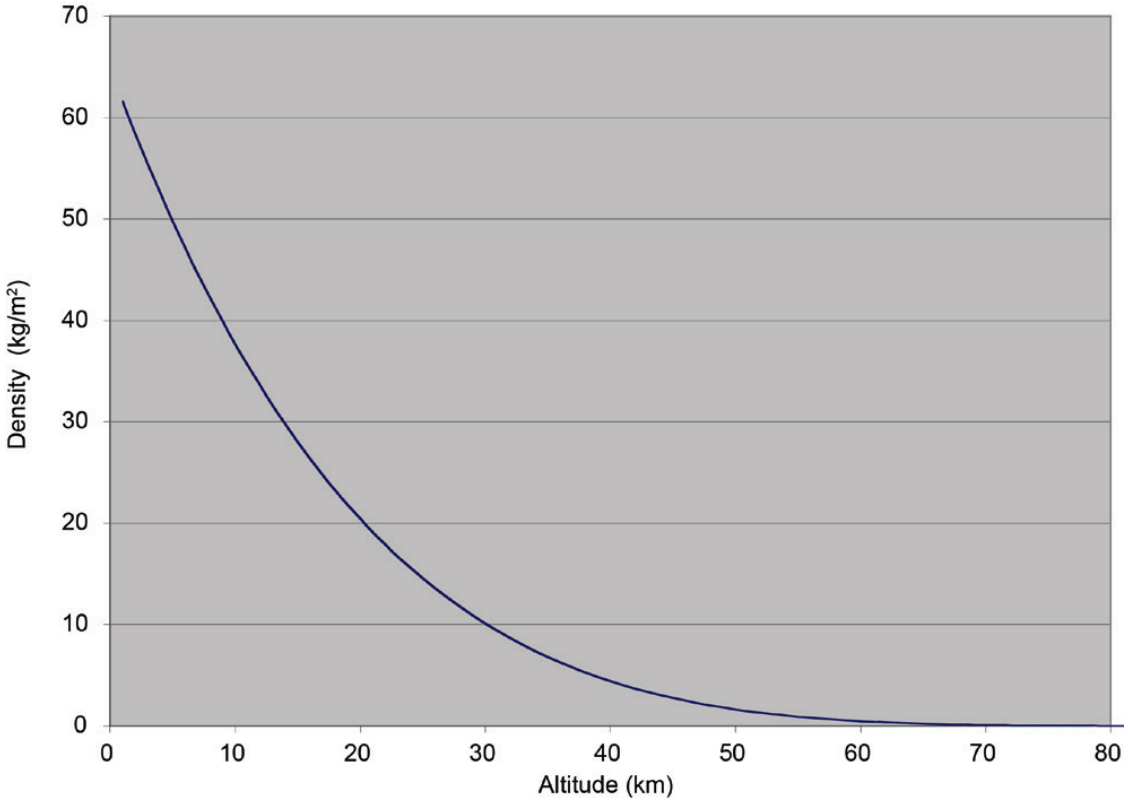

Figure 2.3.—Atmospheric density as a function of altitude (Ref. 7).

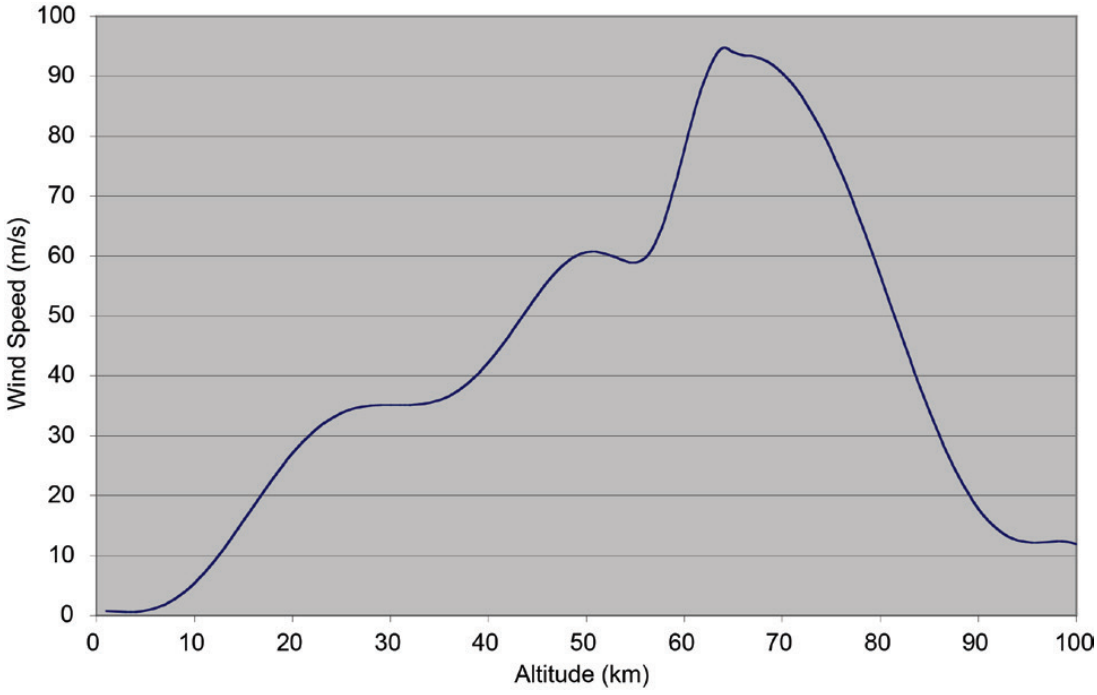

Figure 2.4.—Average wind speed versus altitude within the Venus atmosphere (Ref. 7).

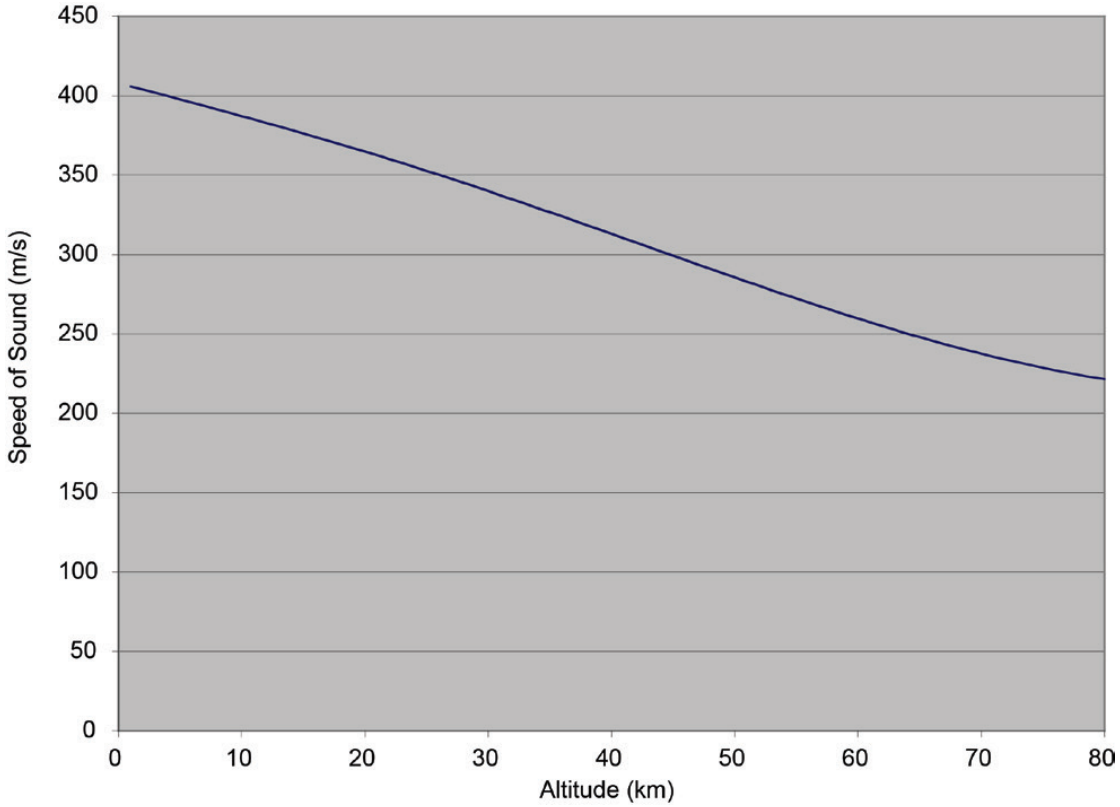

Figure 2.5.—Speed of sound as a function of altitude within the Venus atmosphere (Ref. 7).

The speed of sound (a) in meters per second as a function of altitude above the surface in kilometers can be represented by Equation (2.7) and is shown in Figure 2.5 as a function of altitude. This is based on the speed of sound in CO_2 at the atmospheric pressure at a given altitude. As can be seen in this figure, the speed of sound increases fairly linearly with decreasing altitude from the upper atmosphere to the surface.

$$a = 410.15 - 2.1102z + 0.008751z^2 - 0.00072086z^3 + 1.0136\times10^{-5}z^4 - 3.6825\times10^{-8}z^5 \qquad (2.7)$$

The last properties of the atmosphere that are of interest are the thermal conductivity (k_a) and the specific heat (c_{pa}). For carbon dioxide near the surface the conductivity is 0.588 W/mK and the specific heat is 1181 J/kg K.

3.0 Airship Configuration and Sizing

For flight on Venus the airship is configured similarly to a standard airship that would operate on Earth. The envelope is ellipsoidal with rear fins for stability and control. The equipment and payload are housed in a spherical, insulated pressure vessel. An electric motor and propeller are used for propulsion and a radioisotope power Stirling engine is used to provide electrical power as well as run the cooler for maintaining the interior of the pressure vessel at a temperature in which the electronics and payload can operate. This general layout is shown in Figure 3.1.

Sizing the airship for flight on Venus is an iterative process based on the desired flight altitude and speed. The component masses and sizes are calculated from an initial guess at the required lift and power needed for the airship to operate. From these the actual lift and power requirements are determined. These are compared against the estimated values. If different, then the vehicle size is adjusted and the mass, lift and power is recalculated. This iterative process is continued until the initial and calculated lift and power

values converge. A converged solution represents a design point for the vehicle that meets the selected flight environment and payload requirements. This airship sizing method is illustrated in Figure 3.2.

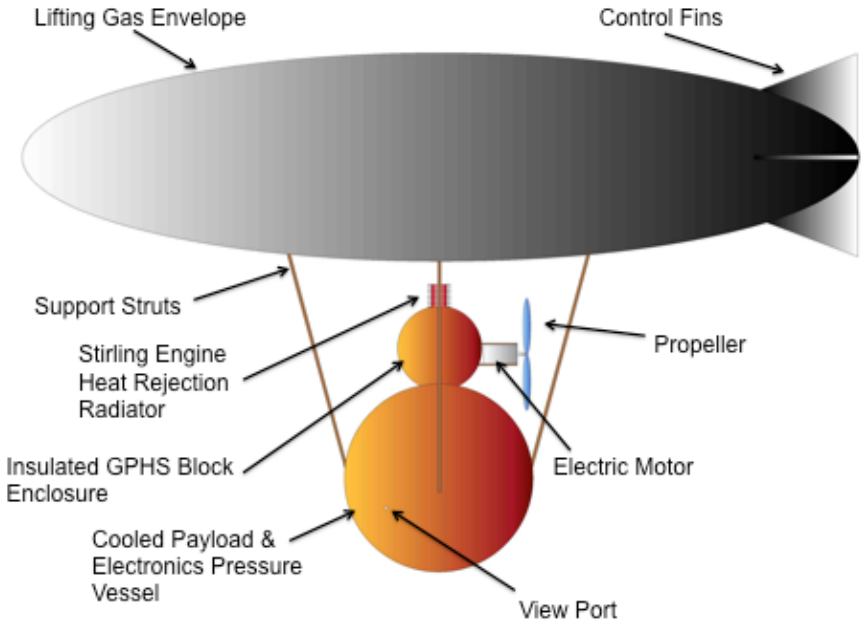

Figure 3.1.—Venus airship main component layout.

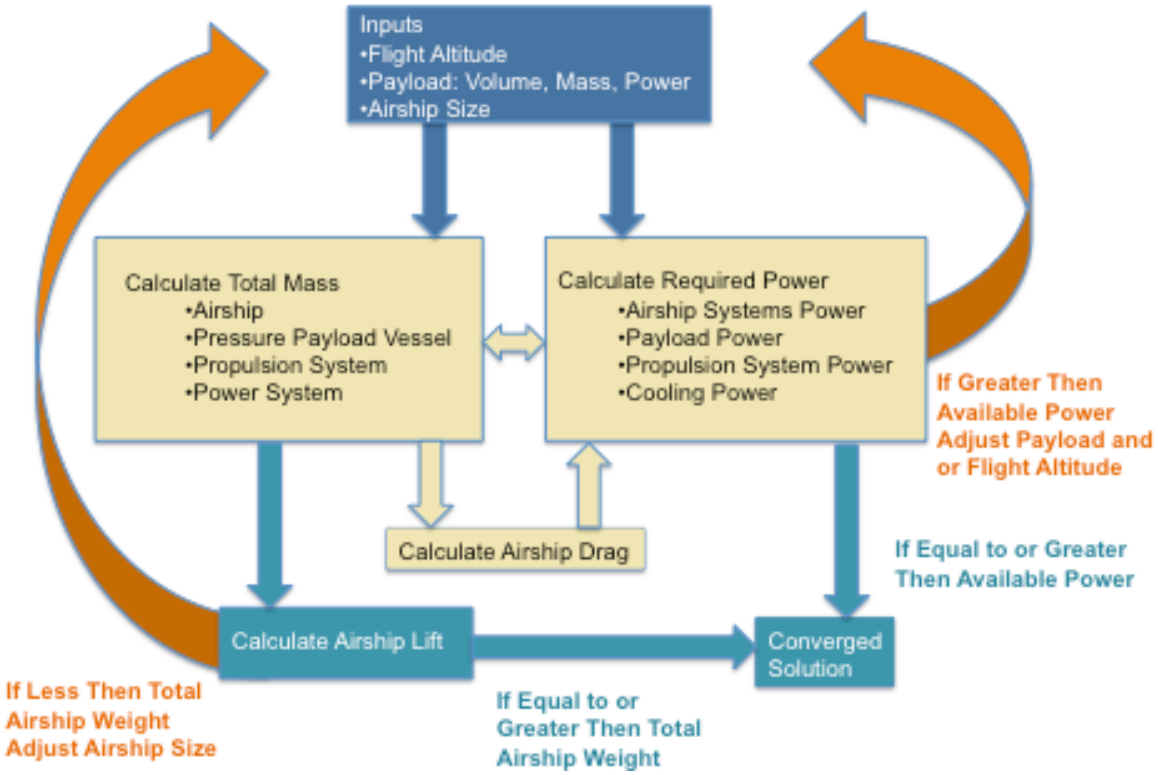

Figure 3.2.—Logic diagram for airship sizing analysis.

3.1 Airship Mass

The total airship mass is the sum of all the components and systems that make up the airship. These components are scaled based on various factors such as power level, size, velocity etc. The components and their associated scaling factors are listed in Table 3.1.

TABLE 3.1.—SCALING AND EFFECT DEPENDENCE OF AIRSHIP COMPONENTS

Component	Scaling Factor	Effect on Airship
Airship Structure: Envelope, Tail, Structural Supports, Lifting Gas	Airship Geometry and Size, Flight Speed, Altitude	Lifting Capability, Drag, Mass
Propulsion Drive Train: Electric Motor, Motor Controller, Gearbox, Power Conditioning, Propeller	Propulsion Power and Thrust, Flight Speed, Altitude	Power Consumption, Flight Velocity, Mass
Stirling Engine System: Stirling Engine, Cooler and Alternator, Pneumatic Coupling, Cooling Fins, GPHS Blocks	Number of GPHS Blocks, Flight Speed, Altitude	Power Availability, Cooling Capability, Mass
Payload and Electronics: Flight Control Computer, Communications Equipment, Payload, Sensors	Inputted Values, Constants	Power Consumption, Mass
Payload/Electronics Enclosure: Pressure Vessel, Insulation, View Port	Interior Volume and Temperature	Mass, Cooling Power

3.1.1 Structure Mass

The airship shape is assumed to be an ellipsoid with its length (l) going from the front tip to the rear tip and the diameter (d) being the maximum thickness in the center of the airship. The fineness ratio (f) of the airship is the ratio of length to diameter as given by Equation (3.1). The length and fineness ratio are used as the input variables to vary the airship size and geometry. The airship volume (V_a) and surface area (S_a) are given by Equations (3.2) and (3.3).

$$f = \frac{l}{d} \tag{3.1}$$

$$V_a = \frac{4\pi l^3}{3f} \tag{3.2}$$

$$S_a = 2\pi\left[\left(\frac{l}{2f}\right)^2 + \left(\frac{l}{2}\right)^2 \frac{\cos^{-1}\left(\frac{1}{f}\right)}{\tan\left(\cos^{-1}\left(\frac{1}{f}\right)\right)}\right] \tag{3.3}$$

The airship structure mass (m_s), given in Equation (3.4), is based on the aerial density (ρ_e, assumed to be 0.25 kg/m^2) of the covering, the number of control fins (n_f) and ratio of fin area to airship volume (R_f) along with a fin structure factor (S_f, assumed to be 1.2) to account to the internal structural support and controls for the fins. In addition a structure factor assumes that the internal structure of the airship envelope scales as 1/4 of the total mass of the airship (m_{tot}) (Ref. 4). This component is added to account for the fixed structure needed to attach components to the envelope.

$$m_s = n_f R_f V_a \rho_e S_f + \frac{m_{tot}}{4} + S_a \rho_a \tag{3.4}$$

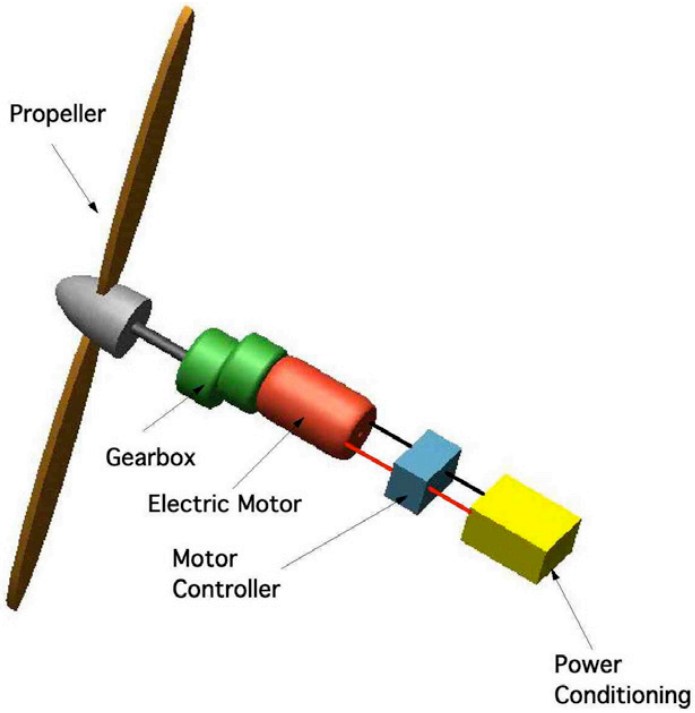

Figure 3.3.—Propulsion system component layout.

3.1.2 Propulsion System Mass

The propulsion system mass consists of the mass of the electric motor (m_{em}), motor controller (m_{mc}), gearbox (m_g), propulsion power conditioning electronics (m_{pc}) and propeller (m_{prop}). The operational efficiency of each of the components of the power system must also be taken into account when sizing the airship. The airship power train is shown in Figure 3.3. The total efficiency of the propulsion system drive train (η_p) , given by Equation (3.5), is composed of the motor controller efficiency (η_{mc}), electric motor efficiency (η_{em}), gearbox efficiency (η_g), power conditioning (η_{pc})and propeller efficiency (η_{prop}).

$$\eta_p = \eta_{mc}\eta_{em}\eta_g\eta_{prop} \tag{3.5}$$

The operational efficiency associated with each of these components is given in Table 3.2. They are combined to get the drive-line efficiency which consists of all components up to the propeller. The propeller efficiency has to be calculated based on a propeller sizing for the operational altitude and thrust requirement. These efficiencies are representative approximations for each of the components under optimized operating conditions.

TABLE 3.2.—DRIVE LINE COMPONENT EFFICIENCIES

Component	Efficiency
Control Electronics	η_{mc} 0.98
Motor	η_{em} 0.90
Gearbox	η_g 0.90
Power Conditioning	η_{pc} 0.98
Drive Line Efficiency	η_p 0.78

Sizing the propeller is an iterative process that is dependent on the airship flight speed and thrust requirement. To achieve the desired thrust at the needed airspeed, the propeller diameter, rpm, and pitch angle are iterated upon. The goal is to provide a combination of these that maximizes efficiency for a

given propeller geometry (airfoil section, blade twist and chord distribution). For this analysis it was assumed that a variable pitch two bladed propeller was utilized. An approximation for the thrust (c_t) and power (c_p) coefficients were derived as a function of advance ratio (J) (Refs. 8 and 9). The thrust and power coefficient equations, (3.6) and (3.7), respectively, are valid for advance ratios within the range of 0.18 to 3.0.

$$c_t = -0.012122 + 0.14577J - 0.1408J^2 + 0.05374J^3 - 0.0068444J^4 \tag{3.6}$$

$$c_p = -0.012752 + 0.094954J - 0.053694J^2 + 0.017534J^3 - 0.0007872J^4 \tag{3.7}$$

The advance ratio, given in Equation (3.8), can be expressed in terms of the flight velocity (U) the speed of sound within the atmosphere (a) and the desired tip Mach number (M).

$$J = \frac{U\pi}{\sqrt{(aM)^2 - U^2}} \tag{3.8}$$

By selecting a tip Mach number, the propeller efficiency can be calculated from the above equations.

$$\eta_{prop} = \frac{c_t J}{c_p} \tag{3.9}$$

The electric motor mass (Refs. 9 and 10), motor controller mass (Refs. 9 and 10), gearbox mass (Refs. 9 and 10), and mass of the power conditioning system (Refs. 9 and 10) are based on a linear scaling with power output (P). The lower-limit at which the equations are valid are listed after each equation. If the required power was sufficiently small so that the calculated mass of any component was below this minimum then the minimum value was used.

$$m_{em} = \frac{P\eta_{mc}}{\eta_p 1291} \qquad \text{(minimum of 0.5 kg)} \tag{3.10}$$

$$m_{mc} = \frac{P}{\eta_p 6233} \qquad \text{(minimum of 0.1 kg)} \tag{3.11}$$

$$m_g = \frac{P\eta_{em}\eta_{mc}}{\eta_p 3278} \qquad \text{(minimum of 0.5 kg)} \tag{3.12}$$

$$m_{pc} = \frac{\eta_p P}{\eta_{pc} 1000} \qquad \text{(minimum of 0.2 kg)} \tag{3.13}$$

The propeller mass is based on the propeller diameter (d_{prop}), given in Equation (3.14), and the number of blades (n_b). The diameter is dependent on the amount of thrust generated by the propeller. This thrust will be equal to the airship drag (D) at the desired flight speed. With the diameter and number of blades known, the mass of the propeller will depend on the volume of each blade, its material density (ρ_{prop}), and the void fraction within the blade (v_b). Using the airfoil cross-sectional area and the chord length distribution given in Reference 8, the volume of the propeller blade (V_{prop}) can be calculated. This volume is given by Equation (3.15) and the total propeller mass is given by Equation (3.16). For this analysis it was assumed that the propeller had two blades and was constructed of carbon composite, with a density of

1380 kg/m^3, and with no void within the blade. Also a 10 percent increase in the total propeller blade mass was added to account for the hub and attachment to the drive shaft.

$$d_{prop} = \sqrt{\frac{D\pi^2}{c_t\left((aM)^2 - U^2\right)}} \tag{3.14}$$

$$V_{prop} = 9.25739 \times 10^{-5} d_{prop}^3 \tag{3.15}$$

$$m_{prop} = 1.1\rho_{prop} n_b (1 - v_b) V_{prop} \tag{3.16}$$

The total propulsion system drive train mass (m_{ps}), given by Equation (3.17), is the sum of the masses from Equations (3.10) through (3.16).

$$m_{dt} = m_{em} + m_{mc} + m_g + m_{pc} + m_{prop} \tag{3.17}$$

3.1.3 Power System Mass

The power generation system provides electrical power to the drive motor as well as to the electronics and payload. It also provides mechanical power for operating the cooler for maintaining the electronics/ payload enclosure at its operating temperature. Electrical power is generated by an isotope powered Stirling engine. The mass breakdown for the power system includes the mass of the Stirling engine (m_{se}, given in Eq. (3.18)), mass of the cooler and alternator (m_{ca} given in Eq. (3.19)), mass of the engine pneumatic coupling (m_{sepc} given in Eq. (3.20)), mass of the radioisotope blocks including their support structure (m_r given in Eq. (3.21)) and mass of the cooling fins (m_f given in Eq. (3.30)). The baseline for this design study used 10 GPHS blocks. Since the number of GPHS blocks (n_r) was predetermined and any variation examined would be near this number of blocks, a linear scaling of the power system components was use. This mass scaling of the components is based on the number of GPHS blocks used. It should be noted that this scaling is only valid for a system using approximately 10 GPHS blocks (±5). The accuracy of the power system mass estimates will diminish as the power level varies from the baseline 10 GPHS blocks.

$$m_{se} = 1.25 n_r \tag{3.18}$$

$$m_{ca} = 1.138 n_r \tag{3.19}$$

$$m_{sepc} = 0.0625 n_r \tag{3.20}$$

$$m_r = 1.44 n_r + 1.2 n_r \tag{3.21}$$

The GPHS blocks are housed in an insulated pressure vessel designed to minimize the heat loss from the blocks to the surrounding atmosphere. This pressure vessel is illustrated in Figure 3.4 and Figure 3.6 for a configuration with 10 GPHS blocks in two stacked groups of five blocks. The mass of the radioisotope heat source pressure vessel (m_{hv}), given by Equation (3.22), is the sum of the masses of the insulation (m_{hi}), inner wall (m_{hwi}) and the outer pressure vessel (m_{hwo}), as illustrated in Figure 3.4 and given by Equations (3.23) through (3.26). The inner wall mass is dependent on its material density (ρ_{hwi}), the inner radius (r_{hi}) of the radioisotope heat source enclosure and its wall thickness (t_{hwi}). The inner wall radius is based on the arrangement of the GPHS blocks. In the configuration illustrated it is set by the height of the two-stacked blocks and their distance from the center of the pressure vessel sphere.

$$m_{hv} = m_{hi} + m_{hwi} + m_{hwo} \tag{3.22}$$

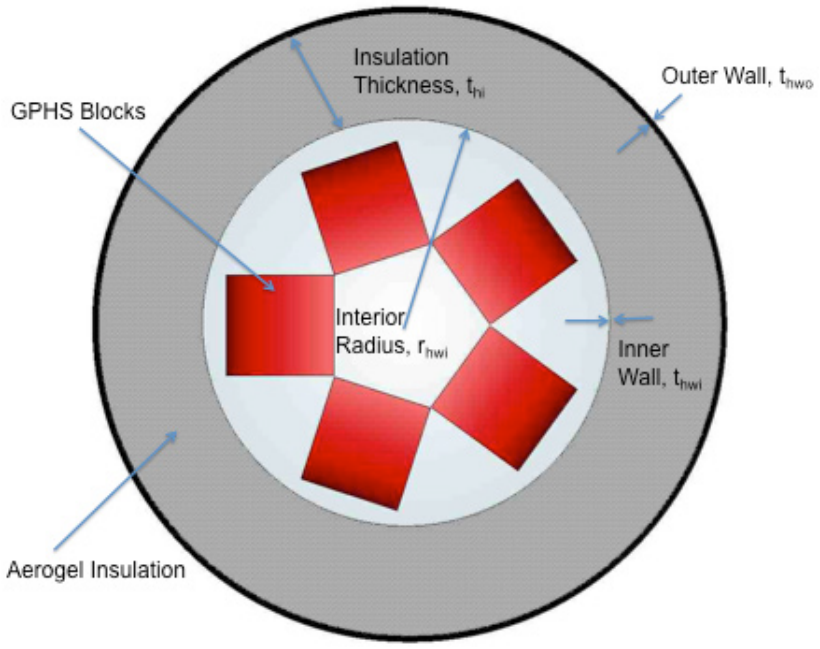

Figure 3.4.—Radioisotope heat source pressure vessel layout.

$$m_{hwi} = \frac{8}{3}\pi\rho_{hwi}t_{hwi}\left(r_{hi}^2 + r_{hi}t_{hwi} + \frac{t_{hwi}^2}{2}\right) \tag{3.23}$$

$$m_{hi} = \frac{4}{3}\pi\rho_i\left[\left(r_{hi} + t_{hwi} + t_{hi}\right)^3 - \left(r_{hi} + t_{hwi}\right)^3\right] \tag{3.24}$$

The outer wall provides the structural barrier between the interior pressure (P_i) and the atmospheric pressure (P_a). The pressure vessel external wall thickness (t_{hwo}) necessary to maintain this pressure difference is given by Equation (3.25) and is dependent on the outer wall material yield strength (σ_{ypo}). The subsequent mass for the heat source outer pressure vessel wall is given by Equation (3.26).

$$t_{hwo} = \frac{2F_S\left(r_{hwi} + t_{hwi} + t_{hi}\right)\left(P_a - P_i\right)}{4\sigma_{yho} + FS\left(P_i - P_a\right)} \tag{3.25}$$

$$m_{hwo} = 4\pi\rho_{hwo}t_{hwo}\left(r_{ho}^2 - t_{hwo}r_{ho} - \frac{t_{hwo}^2}{3}\right) \tag{3.26}$$

Where the outer radius (r_{ho}) is given by Equation (3.27).

$$r_{ho} = r_{hwi} + t_{hwi} + t_{hi} + t_{hwo} \tag{3.27}$$

Cooling fins are sized to remove the waste heat from the Stirling engine and transfer it to the atmosphere. Sizing the cooling fins is an iterative process based on the temperature difference between the engine heat rejection temperature (T_r) and the atmosphere temperature (T_a), the engine heat rejection housing height (l_e) and diameter (d_e), the cooling fin diameter (d_f), the cooling fin thickness (t_f), the number of cooling fins (n_{cf}) and the convective heat transfer coefficient to the surroundings (h_f). These variables are illustrated in Figure 3.5.

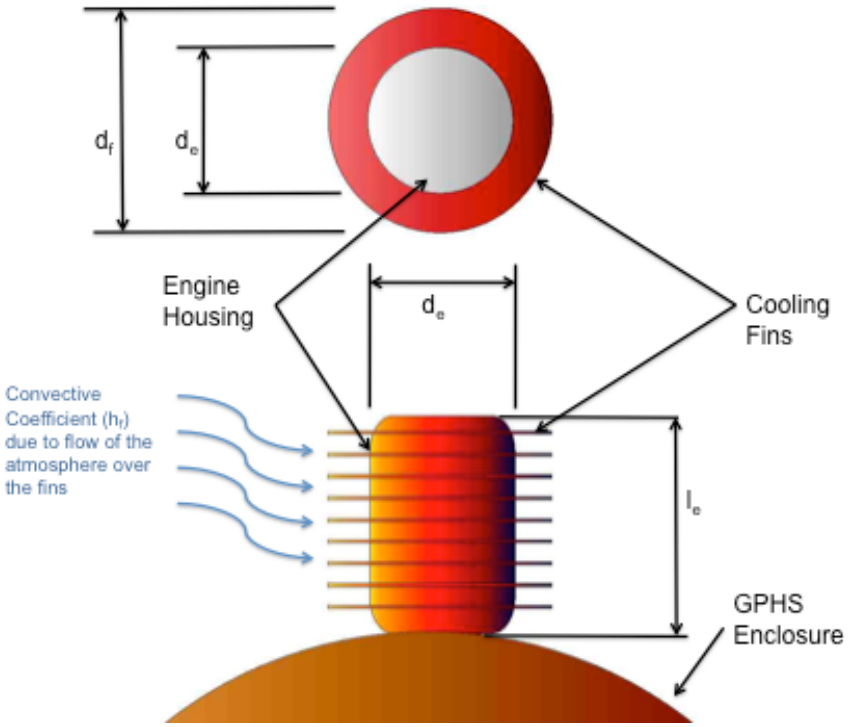

Figure 3.5.—Engine cooling fin geometry.

The heat transfer from each cooling fin (Q_f) is given by Equation (3.28).

$$Q_f = \frac{\pi h_f}{2}\left(d_f^2 - d_e^2\right)\left(T_r - T_a\right) \tag{3.28}$$

The convective heat transfer coefficient for the fins is dependent on the Reynolds number of the flow through the fins Re_f and the corresponding Prandtl (Pr) and Nusselt numbers (Nu_f) given by Equations (3.29), (3.31), and (3.32), respectively (Ref. 12).

$$\mathrm{Re}_f = \frac{\rho_a U d_h}{\mu_a} \tag{3.29}$$

Where the hydraulic diameter (d_h) of the spacing between the fins is given by Equation (3.30).

$$d_h = 2\left(d_f - d_e\right) + \frac{l_e - n_{cf} t_f}{n_{cf} - 1} \tag{3.30}$$

$$\mathrm{Pr} = \frac{c_{pa}\mu_a}{k} \tag{3.31}$$

$$\mathrm{Nu}_f = \frac{\left(\frac{f_f}{8}\right)\mathrm{Re}_f\,\mathrm{Pr}}{1.07 + 12.7\left(\frac{f_f}{8}\right)^{0.5}\left(\mathrm{Pr}^{0.667} - 1\right)} \tag{3.32}$$

The fin friction factor (f_f) used in the calculation of the Nusselt number is based on Reynolds number and given by Equation (3.33).

$$f_f = \left(1.82 \log_{10}\left(\mathrm{Re}_f\right) - 1.64\right)^{-2} \tag{3.33}$$

Using Equations (3.29) through (3.33) the convective heat transfer coefficient for the cooling fins can be determined from Equation (3.34).

$$h_f = \mathrm{Nu}_f \frac{k_a}{d_h} \tag{3.34}$$

In addition to heat rejection from the fins, there is also some heat transferred to the atmosphere from the exterior of the engine heat exchanger housing (Q_h) as given by Equation (3.35).

$$Q_h = \pi d_e l_e h_f \left(T_r - T_a\right) \tag{3.35}$$

To size the cooling fins, the total heat rejection capability of the housing and fins has to be equal to the total waste heat generated (Q_w) by the Stirling engine, as given by Equation (3.36).

$$Q_w = Q_f + Q_h \tag{3.36}$$

By iterating on the fin size and number to satisfy the equality, given above, the size and corresponding mass of the cooling fins, given by Equation (3.37), can be determined, based on the density of the cooling fin material (ρ_f).

$$m_f = n_{cf} \pi \left(d_f^2 - d_e^2\right) t_f \rho_f \tag{3.37}$$

With the size and mass of the cooling fins determined, the total power system mass (m_{ps}), given by Equation (3.38) can be calculated.

$$m_{ps} = m_{se} + m_{ca} + m_{sepc} + m_r + m_f \tag{3.38}$$

3.1.4 Pressure Vessel Mass

The pressure vessel is used to house the electronics and payload. It is composed of an outer wall capable of withstanding the pressure differential between the outside environment and the interior. The pressure vessel interior is designed to operate at 1 bar whereas the exterior surface pressure on Venus is approximately 90 bar. Inside the outer wall is a layer of aerogel insulation. A second structural shell is used as a means of removing heat through a two stage cooler if desired. On the inside of this second structural shell is another layer of aerogel insulation. The layout of the pressure vessel is shown in Figure 3.6.

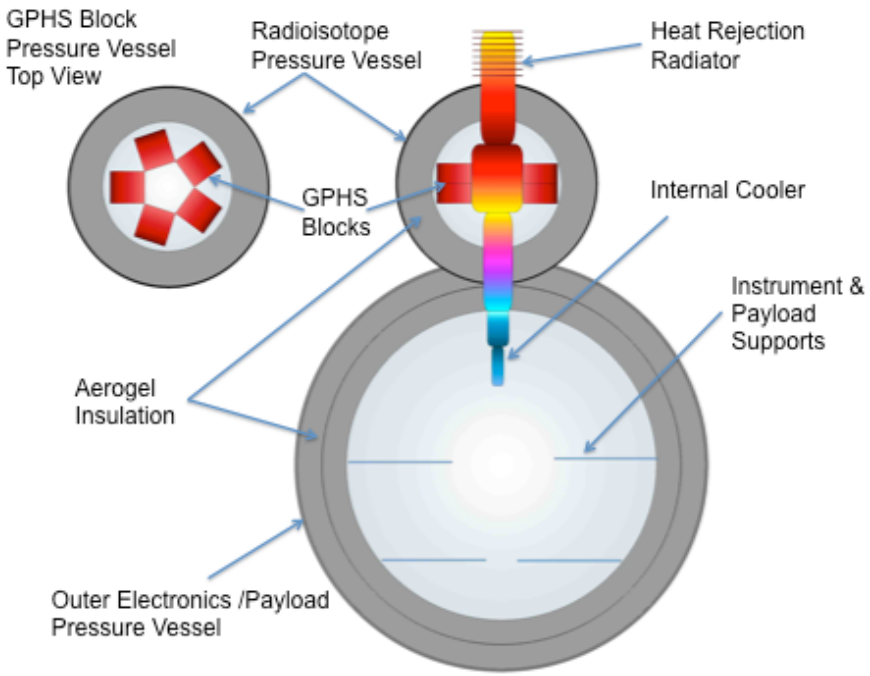

Figure 3.6.—Pressure vessel structure and insulation layout.

The 1 bar internal pressure provides a number of benefits to the system design which include:

- The interior would not have to be evacuated prior to launch.
- Lightweight aerogel can be utilized as the interior insulation.
- Small leaks of atmospheric gas into the interior would not significantly degrade the insulation's insulating ability over a system designed for vacuum operation.
- Internal convection can be used to evenly distribute the internal cooling.

The mass of each layer of the pressure vessel is based on its thickness, surface area and material density. The thickness (t_{po}) of the outer shell wall has to be able to withstand the pressure difference between the atmospheric pressure and the interior pressure. The thickness can be calculated for a specified material based on its yield strength and the desired interior radius (r_{pi}) plus the thickness of the inner and outer insulation layers (t_{ii}, t_{io}) and interior wall structure, as illustrated in Figure 3.7. A factor of safety (F_S) is also used so that the stress at the operational conditions is sufficiently below the yield stress of the material. The pressure vessel exterior wall thickness (t_{po}) is given by Equation (3.39). Using this thickness and the material density of the outer wall (ρ_{po}), its mass is calculated by Equation (3.40).

$$t_{po} = \frac{2F_S\left(r_{pi} + t_{ii} + t_{io} + t_{pi} + t_{pm}\right)\left(P_a - P_i\right)}{4\sigma_{ypo} + F_S\left(P_i - P_a\right)} \tag{3.39}$$

$$m_{po} = 4\pi\rho_{po}t_{po}\left(r_{po}^2 - t_{po}r_{po} - \frac{t_{po}^2}{3}\right) \tag{3.40}$$

The outer radius of the pressure vessel (r_{po}) is given by Equation (3.41).

$$r_{po} = r_{pi} + t_{pi} + t_{ii} + t_{pm} + t_{io} + t_{po} \tag{3.41}$$

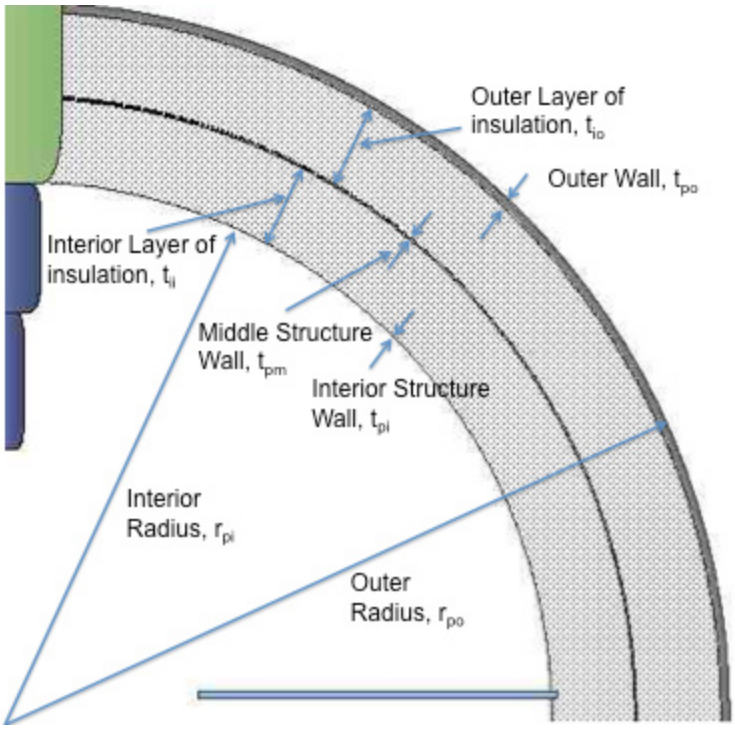

Figure 3.7.—Interior layers of the pressure vessel.

The mass of the middle (m_{pm}) and inner (m_{pi}) structural layers are also calculated based on their thickness (t_{pm} and t_{pi}, respectively), material density (ρ_{pm}, ρ_{pi}, respectively) and surface area, as given by Equations (3.42) and (3.43), respectively. However, since there is no structural load on the middle and inner walls, the thickness was provided as an input and not calculated.

$$m_{pm} = \frac{4}{3}\pi\rho_{pm}\left[\left(r_{pi} + t_{pi} + t_{ii} + t_{pm}\right)^3 - \left(r_{pi} + t_{pi} + t_{ii}\right)^3\right] \tag{3.42}$$

$$m_{pi} = \frac{8}{3}\pi\rho_{pi}t_{pi}\left(r_{pi}^2 + r_{pi}t_{pi} + \frac{t_{pi}^2}{2}\right) \tag{3.43}$$

The last component mass of the pressure vessel is the inner (m_{ii}) and outer (m_{io}) insulation layers. The orientation of these layers is shown in Figure 3.8. Both layers are inside the outer pressure vessel wall and are therefore at the interior pressure. The insulation layer thickness is a variable that can be adjusted during the design process to control the heat leak from the atmosphere into the pressure vessel and therefore control the required cooling power. The corresponding mass of the insulation layers is based on the insulation density (ρ_i) and thickness, given by Equations (3.44) and (3.45).

$$m_{ii} = \frac{4}{3}\pi\rho_i\left[\left(r_{pi} + t_{pi} + t_{ii}\right)^3 - \left(r_{pi} + t_{pi}\right)^3\right] \tag{3.44}$$

$$m_{io} = \frac{4}{3}\pi\rho_i\left[\left(r_{pi} + t_{pi} + t_{ii} + t_{pm} + t_{io}\right)^3 - \left(r_{pi} + t_{pi} + t_{ii} + t_{pm}\right)^3\right] \tag{3.45}$$

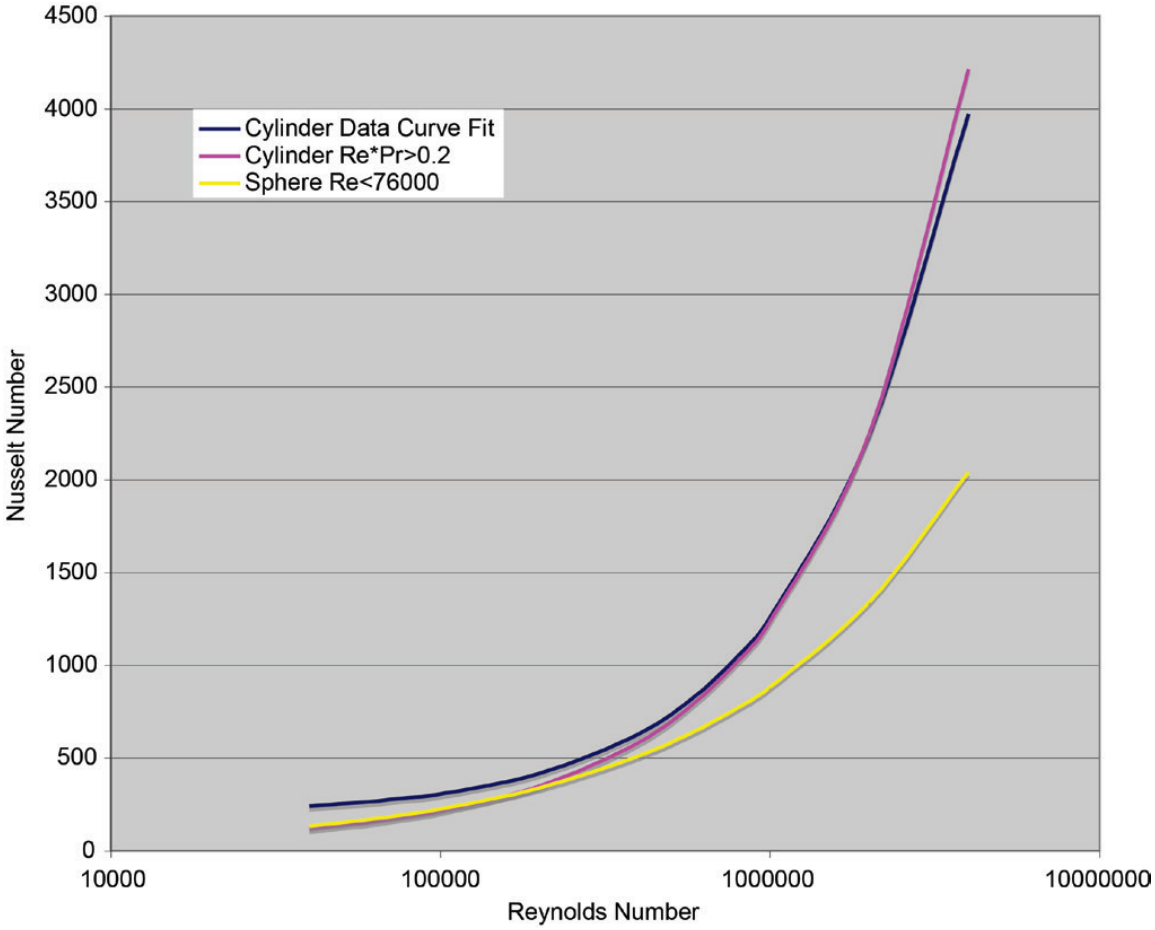

Figure 3.8.—Nusselt number as a function of Reynolds number for cross flow over cylinder and a sphere.

The total mass of the pressure vessel (m_p), given by Equation (3.46), is the sum of the masses from Equations (3.40) through (3.45). An additional 10 percent margin is added to the total mass to account for items such as internal structure and miscellaneous hardware.

$$m_p = 1.1\left(m_{po} + m_{pm} + m_{pi} + m_{ii} + m_{io}\right) \tag{3.46}$$

The last component is the structural supports that hold the pressure vessel to the airship envelope. The struts are composed of solid circular cylinders. The mass of the struts, given by Equation (3.47), is dependent on the strut material density (ρ_{ss}), number of struts (n_{ss}), strut length (l_s) and diameter (d_{ss}). It was assumed that the struts would connect to the centerline of the payload pressure vessel and would extend to the base of the envelope as shown in Figure 3.1. The length of the struts is based on the diameters of the payload and heat source pressure vessels, the height of the engine heat exchanger and its spacing from the bottom of the lifting gas envelope. As with the pressure vessel there is a 10 percent margin added onto the struts to account for additional material at the attachment points.

$$m_{ss} = 1.1\pi\left(\frac{d_s}{2}\right)^2 l_s n_s \rho_s \tag{3.47}$$

The lifting gas mass (m_{lg}), given by Equation (3.48), also factors into the total airship mass. Its mass is dependent on the lifting gas molecular weight (M_{Wg}), temperature and pressure and the airship gas volume. The universal gas constant (R) has a value of 0.0831 m^3Bar/kMol K and it is assumed the gas is at atmospheric conditions.

$$m_{\lg} = \frac{M_{W\,g} V_a P_a}{T_a R} \tag{3.48}$$

3.1.5 Total Mass

The last series of components that have to be accounted for in determining the total mass of the airship are fixed and do not scale with the airship size. These fixed mass components are listed in Table 3.3.

TABLE 3.3.—AIRSHIP FIXED COMPONENT MASSES

Component	Mass, kg	Power, W
Flight Control Computer (m_{fc}, P_{fcc})	3.8	10
Communications Equipment (m_{ce} , P_{ce})	4.6	19
Flight Control Sensors (m_{fs}, P_{fcs})	3.5	9
Payload (m_{pl}, P_{pl})	25.0	19

The sum of these fixed mass items is given by Equation (3.49).

$$m_{fi} = m_{fc} + m_{ce} + m_{fs} + m_{pl} \tag{3.49}$$

From the above equations the total airship mass (m_{tot}), given by Equation (3.50), can be calculated.

$$m_{tot} = m_s + m_{dt} + m_{ps} + m_p + m_{hv} + m_{ss} + m_{\lg} + m_{fi} \tag{3.50}$$

Determining the total airship mass and subsequent gas envelope size is an iterative process. The airship envelope volume, given by Equation (3.2), determines the total weight that the airship can lift. The lifting force (L) of the airship is based on a centuries old principle discovered by Archimedes, “A body wholly or partly immersed in a fluid is buoyed up with a force equal to the weight of the fluid displaced by the body”. This principle is expressed by Equation (3.51), which is dependent on the gravitational force on Venus (g =8.93 m/s^2), the ratio of the molecular weights of the lifting gas and the atmosphere (M_{Wa}), the density of the atmosphere and the gas constant of the atmosphere (R_a=188.92 J/kg-K). This equation assumes that the pressure within the lifting gas envelope is the same as that of the atmosphere and unless the lifting gas is actively heated, its temperature (T_g) will also be the same as that of the atmosphere. This equation also takes into account the lift that would be generated by the payload and GPHS block enclosures due to their internal pressure being lower than the atmospheric pressure.

$$L = \left[\rho_a V_a \left(1 - \frac{M_{Wg} T_a}{M_{Wa} T_g} \right) + \frac{4}{3} \pi \left(r_{pi}^3 \left(\rho_a - \frac{P_i}{R_a T_i} \right) + r_{hwi}^3 \left(\rho_a - \frac{P_i}{R_a T_h} \right) \right) \right] g \tag{3.51}$$

The total lifting force is then compared to the total weight of the airship (W_{tot}), as given by Equation (3.52). In the analysis the envelope size is then iterated on until the lifting force is greater than or equal to the airship weight.

$$W_{tot} = g m_{tot} \tag{3.52}$$

3.2 Power Required

The next step in sizing the airship is determining the total power required to fly and operate the airship and payload systems. Determining this is an iterative process between the sizing of the airship to lift its mass and the power needed to overcome drag due to its size and shape along with the power needed to provide cooling to the pressure vessel. As with the total mass, the total power will be a summation of the power required by the various systems of the airship given by Equation (3.53). The main power consuming items on the airship is propulsion and cooling (P_c).

$$P_r = P_{fc} + P_{ce} + P_{fs} + P_{pl} + P + P_c \tag{3.53}$$

3.2.1 Propulsion Power

The propulsion power required by the airship to fly at a specified velocity is given by Equation (3.54).

$$P = \frac{DU}{\eta_p} \tag{3.54}$$

The total airship drag is the summation of the drag of each component exposed to the atmosphere flow over the airship as it moves. The main airship structure containing the lifting gas can be broken into two segments, the gas envelope and the tail section with control fins. The lifting gas envelope drag (D_e), given by Equation (3.55) is based on the airship's velocity, the volume of the lifting gas and its drag coefficient (c_{de}).

$$D_e = \frac{1}{2}\rho_a U^2 c_{de} V_a^{\frac{2}{3}} \tag{3.55}$$

The gas envelope drag coefficient is based on the fineness ration for the airship and is given by Equation (3.56). This equation represents a curve fit to drag coefficient data for various airship fineness ratios (Ref. 13).

$$c_{de} = 0.2318 - 0.1576 f + 0.04744 f^2 - 0.007041 f^3 + 5.135\times10^4 f^4 - 1.48\times10^5 f^5 \tag{3.56}$$

The tail section drag (D_t) is scaled linearly from the lifting gas envelope drag as given by Equation (3.57) (Ref. 13).

$$D_t = 0.167 D_e \tag{3.57}$$

The next main drag components are for the pressure vessels. Since the pressure vessels for the electronics/payload is similar to that for the heat source the drag for each (D_p and D_h respectively) is calculated in a similar manner. The main electronics/payload pressure vessel drag is given by Equation (3.58), and that for the heat source enclosure is given by Equation (3.59).

$$D_p = \frac{\pi}{2}\rho_a U^2 c_{dpv} r_{po}^2 \tag{3.58}$$

$$D_h = \frac{\pi}{2}\rho_a U^2 c_{dpv} r_{ho}^2 \tag{3.59}$$

The drag coefficient for either pressure vessel (c_{dpv}) is dependent on the flow Reynolds number. The drag coefficient for a sphere is given by Equation (3.60) and the coefficients are given in Table 3.4 for

different ranges of Reynolds number (Re_{pv}), given by Equation (3.61), for the pressure vessel based on its diameter (d_{pv}). These are based on a curve fit from experimental data (Ref. 12).

$$c_{dpv} = c_{0s} + c_{1s}\,\mathrm{Re}_{do} + c_{2s}\,\mathrm{Re}_{do}^2 \tag{3.60}$$

$$\mathrm{Re}_{do} = \frac{\rho_a U d_{pv}}{\mu_a} \tag{3.61}$$

TABLE 3.4.—SPHERICAL PRESSURE VESSEL DRAG COEFFICIENT CONSTANTS

Reynolds Number Range	c_{0s}	c_{1s}	c_{2s}
$\mathrm{Re}_{pv} <= 100$	3.6279	-0.045484	1.9292×10^{-4}
$100 < \mathrm{Re}_{pv} <= 1000$	0.92	-7.08×10^{-4}	2.40×10^{-7}
$1000 < \mathrm{Re}_{pv} <= 1\times10^4$	0.4675	-7.80×10^{-6}	4.00×10^{-10}
$1\times10^4 < \mathrm{Re}_{pv} <= 1\times10^5$	0.43	4.00×10^{-7}	0.00
$1\times10^5 < \mathrm{Re}_{pv} <= 1\times10^6$	0.19	1.80×10^{-6}	-2.56×10^{-12}
$1\times10^6 < \mathrm{Re}_{pv} <= 1\times10^7$	0.10167	9.00×10^{-9}	-6.67×10^{-16}

The drag for the heat exchanger (D_{he}), shown in Figure 3.5, is given by Equation (3.62). The first part of the equation provides the drag for the cooling fins and the second part is the drag of the main heat exchanger cylinder.

$$D_{he} = \frac{\rho_a f_f U^2 l_e d_f^2}{2 d_h} + \frac{\rho_a U^2 l_e d_e c_{dhe}}{2} \tag{3.62}$$

As with the pressure vessel, the drag coefficient for the heat exchanger (c_{dhe}, given by Eq. (3.63)) is a function of the Reynolds number for the flow over its surface (given in Eq. (3.29)). The heat exchanger drag coefficient also includes an adjustment factor to account for the aspect ratio (length to diameter) for the cylinder (Refs. 12and 14).

$$c_{dhe} = \left(c_{0c} + c_{1c}\,\mathrm{Re}_f + c_{2c}\,\mathrm{Re}_f^2\right)\left(0.0787 \ln\left(\frac{l_e}{d_e}\right) + 0.5143\right) \tag{3.63}$$

As discussed previously there are four cylindrical struts used to hold the pressure vessels and the other components to the gas envelope. The drag for these struts (D_s) is given by Equation (3.64). Since the struts are cylindrical in shape the coefficients used in Table 3.5 can be used to calculate the drag coefficient (c_{ds}) for the struts based on the Reynolds number (Re_s) of the flow around them.

$$D_s = \frac{1}{2} n_s \rho_a U^2 l_s d_s c_{ds} \tag{3.64}$$

$$c_{ds} = \left(c_{0c} + c_{1c}\,\mathrm{Re}_s + c_{2c}\,\mathrm{Re}_s^2\right)\left(0.0787 \ln\left(\frac{l_s}{d_s}\right) + 0.5143\right) \tag{3.65}$$

$$\mathrm{Re}_s = \frac{\rho_a U d_s}{\mu_a} \tag{3.66}$$

TABLE 3.5.—INFINITE CYLINDER DRAG COEFFICIENT CONSTANTS

Reynolds Number Range	c_{0c}	c_{1c}	c_{2c}
$Re_{pv} <= 100$	3.5645	–0.04215	2.088×10^{-4}
$100 < Re_{pv} <= 1000$	1.4464	-7.241×10^{-4}	2.92×10^{-7}
$1000 < Re_{pv} <= 1\times10^{4}$	1.0191	-2.21×10^{-5}	3.18×10^{-9}
$1\times10^{4} < Re_{pv} <= 1\times10^{5}$	1.0897	5.34×10^{-6}	-4.01×10^{-11}
$1\times10^{5} < Re_{pv} <= 1\times10^{6}$	1.4263	-1.18×10^{-6}	1.00×10^{-14}
$1\times10^{6} < Re_{pv} <= 1\times10^{7}$	0.32731	2.76×10^{-8}	-5.46×10^{-16}

From these components the total drag (D_{tot}) for the airship can be determined, as given by Equation (3.67).

$$D_{tot} = D_e + D_t + D_p + D_h + D_{he} + D_s \tag{3.67}$$

3.2.2 Cooling Power

The cooling power for maintaining the desired operating temperature for the electronics/payload enclosure is the largest power-consuming item. The required cooling power is dependent on the heat loss through the electronics/payload pressure vessel to the surroundings. For a single stage cooling system the heat loss (Q_p) through the insulation and pressure vessel walls is given by Equation (3.68). It is based on the temperature difference between the interior and exterior and the thermal resistance for each layer of material within the pressure vessel and the thermal resistances associated with the natural convection within the pressure vessel and the convection from its exterior.

$$Q_p = \frac{T_a - T_i}{R_{ci} + R_{wi} + R_{ii} + R_{wm} + R_{io} + R_{wo} + R_{co}} \tag{3.68}$$

The thermal resistance (R_t) terms for the different material layers that comprise the pressure vessel are all similar and are based on the inner (r_i) and outer (r_o) radius of the layers as well as the layer thermal conductivity (k_m) of the layer material, as given by Equation (3.69).

$$R = \frac{1}{4\pi k_m}\left(\frac{1}{r_i} - \frac{1}{r_o}\right) \tag{3.69}$$

The values, used for the corresponding thermal resistance variables in Equation (3.69), are given in Table 3.6.

TABLE 3.6.—THERMAL RESISTANCE VALUES FOR EACH MATERIAL LAYER IN THE PAYLOAD PRESSURE VESSEL

Resistance Term, R_t	Thermal Conductivity, k_m	Inner Radius, r_i	Outer Radius, r_o
Inner Wall (R_{wi})	k_{wi}	r_{pi}	$r_{pi} + t_{pi}$
Inner Layer of Insulation (R_{ii})	k_{ii}	$r_{pi} + t_{pi}$	$r_{pi}+ t_{pi} + t_{ii}$
Middle Wall (R_{wm})	k_{wm}	$r_{pi} + t_{pi} + t_{ii}$	$r_{pi}+ t_{pi} + t_{ii} + t_{pm}$
Outer Layer of Insulation (R_{io})	k_{io}	$r_{pi} + t_{pi} + t_{ii} + t_{pm}$	$r_{pi}+ t_{pi}+ t_{ii}+ t_{pm} + t_{io}$
Outer Wall (R_{wo})	k_{wo}	$r_{pi} + t_{pi} + t_{ii} + t_{pm} + t_{io}$	r_{po}

The remaining two resistance terms are due to the internal convection within the pressure vessel (R_{ci}) and the external convection (R_{co}) to the atmosphere. These are given by Equations (3.70) and (3.71), respectively. These thermal resistances are dependent on the internal (h_i) and external (h_o) convection coefficients.

$$R_{ci} = \frac{1}{4\pi h_i r_{pi}^2} \tag{3.70}$$

$$R_{co} = \frac{1}{4\pi h_o r_{po}^2} \tag{3.71}$$

Determining the convection coefficients for each of the convection thermal resistance terms is a key aspect in accurately calculating the heat leak through the walls and insulation of the pressure vessel. The convection coefficients for both the interior and exterior convection are given by Equations (3.72) and (3.73), respectively. These coefficients are determined by utilizing the geometry and gas properties at each location. The main factor in calculating the convective coefficients is in determining the Nusselt number for each location.

$$h_i = \frac{k_i \mathrm{Nu}_{di}}{2r_{pi}} \tag{3.72}$$

$$h_o = \frac{k_a \mathrm{Nu}_{do}}{2r_{po}} \tag{3.73}$$

For calculating the internal convective coefficient the interior gas was assumed to be CO_2 at 1 atm. The thermal conductivity for this gas (k_i) is given by Equation (3.74), which is based on the interior wall film temperature (T_{if}). The internal convective heat transfer is assumed to be natural convection with no active mixing of the gas within the pressure vessel. Therefore there will be a boundary layer with a temperature gradient between the interior wall and the internal gas. The film layer temperature is the average of the interior temperature and the wall temperature. The difference between the wall and the interior gas temperature (ΔT_{wi}) was assumed to be 10 °C with a baseline internal temperature of 320 K.

$$k_i = -0.0091 + 8.79\times10^{-5} T_{if} - 9.03\times10^{-9} T_{if}^2 \qquad \{\mathrm{W/m\ K}\} \tag{3.74}$$

The internal gas Nusselt number (Nu_{di}) for internal free convection within the pressure vessel is given by Equation (3.75) (Ref. 11).

$$\mathrm{Nu}_{di} = 0.18\left(\frac{\mathrm{Pr}_i\, Ra_i}{0.2 + \mathrm{Pr}_i}\right)^{0.29} \tag{3.75}$$

The pressure vessel internal gas Prandtl number (Pr_i) is based on the internal gas specific heat (c_{pi}), thermal conductivity and dynamic viscosity (μ_i) of the gas as defined by Equation (3.76).

$$\mathrm{Pr}_i = \frac{c_{pi}\mu_i}{k_i} \tag{3.76}$$

To calculate the Prandtl number for the internal gas the thermal conductivity is given by Equation (3.74) and the specific heat and dynamic viscosity is given by Equations (3.77) and (3.78), respectively as a function of the wall film temperature.

$$c_{pi} = 0.509 + 0.00134 T_{if} - 6.46\times10^{-7} T_{if}^2 \qquad \{\mathrm{kJ/kg\ K}\} \tag{3.77}$$

$$\mu_i = 4.69\times10^{-7} + 5.13\times10^{-8}T_{if} - 1.21\times10^{-11}T_{if}^2 \qquad \{\text{kg/m s}\} \tag{3.78}$$

The last factor in calculating the Nusselt number is the determination of the Rayleigh number for the pressure vessel internal gas (Ra_i), defined in Equation (3.78). The Rayleigh number is based on the interior wall film temperature, the kinematic viscosity (ν_i, given by Eq. (3.80)) and the thermal diffusivity (α_i, given by Eq. (3.81)) of the internal gas.

$$Ra_i = \frac{8g\Delta T_{wi} r_{pi}^3}{T_{if}\nu_i\alpha_i} \tag{3.79}$$

$$\nu_i = -3.2\times10^{-6} + 2.03\times10^{-8}T_{if} + 5.95\times10^{-11}T_{if}^2 \qquad \{\text{m}^2/\text{s}\} \tag{3.80}$$

$$\alpha_i = -6.18\times10^{-6} + 3.24\times10^{-8}T_{if} + 8.1\times10^{-11}T_{if}^2 \qquad \{\text{m}^2/\text{s}\} \tag{3.81}$$

The convective coefficient for the flow over the exterior of the pressure vessel is given by Equation (3.73). Unlike the interior, the convective heat transfer for the flow over the exterior of the pressure vessel is forced convection. Therefore, the Nusselt number calculation will be different than that for the interior. Calculating the Nusselt number for the exterior flow is somewhat difficult due to the very high Reynolds number of the flow over the exterior of the sphere.

At flight speeds near the wind velocity of 1 to 2 m/s the Reynolds number, as given by Equation (3.66), is on the order of 3 million. There were no available correlations found for the Nusselt number for flow over a sphere at a Reynolds number in this range. The closest Nusselt number correlation found for flow over a sphere is valid only up to a Reynolds number of 78,000 (Ref. 15), this correlation is graphed in Figure 3.8. A curve fit of data (Ref. 16) on the Nusselt number for flow over a cylinder within a Reynolds number range of $3\times10^4 < \text{Re}_p < 4\times10^6$ is also graphed on Figure 3.9. In addition to the data, Equation (3.82) also represents the Nusselt number as a function of Reynolds number for a cylinder in a cross-flow (Ref. 17).This equation is valid for the product of Prandtl and Reynolds numbers greater than 0.2 ($\text{PrRe}_d > 0.2$).

$$\text{Nu}_{do} = 0.3 + \frac{0.62\,\text{Re}_{do}^{0.5}\,\text{Pr}^{1/3}}{\left[1+\left(\frac{0.4}{\text{Pr}}\right)^{2/3}\right]^{0.25}}\left[1+\left(\frac{\text{Re}_{do}}{282000}\right)^{0.625}\right]^{0.8} \tag{3.82}$$

The valid Reynolds number range for the cross-flow cylinder Nusselt number curves is within the values encountered for flow over the payload pressure vessel near the surface of Venus. Also the Nusselt number for a sphere within the Reynolds number range in which it is valid, is very close to that given by Equation (3.82) for a cylinder in cross-flow (as can be seen on Figure 3.8). Therefore Equation (3.82) was used to approximate the Nusselt number for flow over the spherical pressure vessel. With this expression for Nusselt number, the convective coefficient for the atmosphere flow around the pressure vessel, given by Equation (3.73), can be calculated and in turn the exterior convective resistance term, given by Equation (3.71).

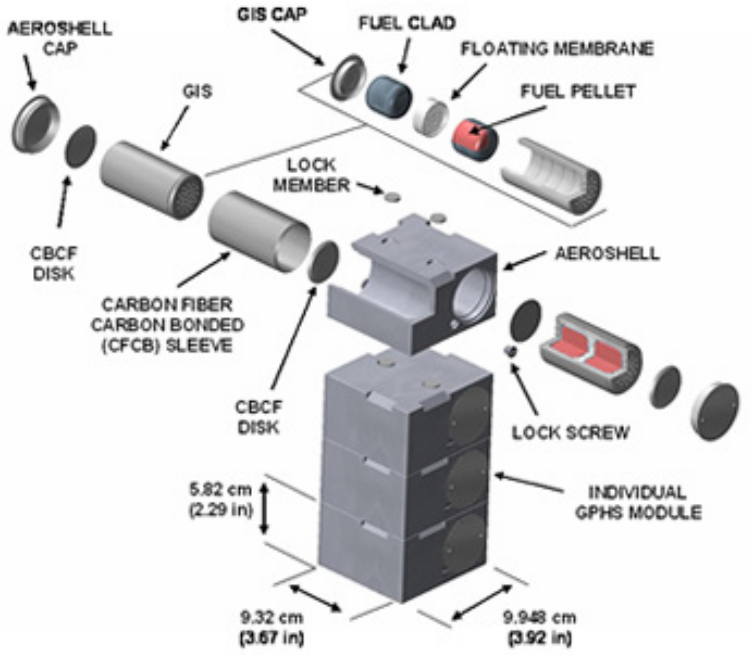

Figure 3.9.—GPHS block assembly drawing (Ref. 18).

The Stirling cooler has to not only remove the heat leaking in through the insulation, but also the wires and view port as well as the heat internally generated by the computer control system and payload. The heat leak through the pass-through wires and view port windows (Q_{pw} and Q_{vp} respectively) is depending on the number of wires (n_w) and view ports (n_{vp}), their diameter (d_w, d_{vp}) and the thermal conductivity of the wire (k_w) or viewport (k_{vp}). The heat leak through the wires and view ports is given by Equations (3.83) and (3.84), respectively.

$$Q_{pw} = \frac{\pi n_w d_w^2 k_w \left(T_a - T_i\right)}{4\left(r_{po} - r_{pi}\right)} \tag{3.83}$$

$$Q_{vp} = \frac{\pi n_{vp} d_{vp}^2 k_{vp} \left(T_a - T_i\right)}{4\left(r_{po} - r_{pi}\right)} \tag{3.84}$$

From Equations (3.68) through (3.84) the total required cooling power could be determined. This required power is the sum of the internal heat that must be removed divided by the efficiency of the Stirling cooler (η_c), as given by Equation (3.85). The cooler efficiency was assumed to be 44 percent.

$$P_c = \frac{\left(P_{fc} + P_{fs} + P_{pl} + Q_p + Q_{pw} + Q_{vp}\right)}{\eta_c} \tag{3.85}$$

3.3 Power Production

The last area to model in sizing the airship is the amount of power available from the Stirling radioisotope powered engine. The Stirling engine converts heat from the isotope blocks to provide electrical and mechanical power. Each radioisotope block, termed a GPHS, provides 250 W of thermal power at their beginning of life. The blocks are comprised of a number of plutonium-238 pellets, as illustrated in Figure 3.9. Each block measures 9.948- by 9.32- by 5.82-cm and has a mass of 1.44 kg.

The blocks are arranged in a circular fashion around the heater head of the engine as illustrated in Figure 3.4 and Figure 3.6. The GPHS blocks are enclosed in an insulated pressure vessel similar to that used for the electronics and payload. The insulated pressure vessel is necessary in order to limit heat loss from the blocks to the surroundings. The heat loss from the GPHS pressure vessel (Q_{hs}) is given by Equation (3.86).

$$Q_{hs} = \frac{T_h - T_a}{R_{ci} + R_{wi} + R_{ii} + R_{wo} + R_{co}} \tag{3.86}$$

The thermal resistance terms for the different material layers that comprise the heat source pressure vessel are all similar to those used for the payload pressure vessel, given by Equation (3.69). The corresponding values for the heat source pressure vessel to be used with Equation (3.69) are given in Table 3.7. Since the heat source pressure vessel has only one layer of insulation only the inner insulation resistance term is used in Equation (3.86).

TABLE 3.7.—THERMAL RESISTANCE VALUES FOR EACH MATERIAL LAYER IN THE HEAT SOURCE PRESSURE VESSEL

Resistance Term, R	Thermal Conductivity k	Inner Radius, r_i	Outer Radius, r_o
Inner Wall (R_{wi})	k_{hwi}	r_{hi}	$r_{hi} + t_{hwi}$
Insulation Layer (R_{ii})	k_{hi}	$r_{hi} + t_{hwi}$	$r_{hi} + t_{hwi} + t_{hi}$
Outer Wall (R_{wo})	k_{hwo}	$r_{hi} + t_{hwi} + t_{hi}$	$r_{hi} + t_{hwi} + t_{hi} + t_{hwo}$

The interior and exterior convective thermal resistance terms for the heat source pressure vessel are calculated in the same manner as those for the payload pressure vessel, given by Equations (3.70) and (3.71), respectively. The inner (r_{hi}) and outer (r_{ho}) radius for the heat source pressure vessel is substituted for those of the payload pressure vessel. The convective coefficients for the heat source pressure vessel are calculated in a similar manner as those for the payload pressure vessel. Since the heat source pressure vessel is operating with the same internal gas and pressure as that of the electronics enclosure, the inner and outer convective coefficients can be determined from Equations (3.72) through (3.82) by substituting in the appropriate dimensions for the heat source pressure vessel in place of those for the electronics pressure vessel and using a baseline internal operating temperature of 1473 K.

To determine the heat available to the engine (Q_e), the heat loss to the environment from the heat source pressure vessel is subtracted from the total heat available from the GPHS blocks, as given by Equation (3.87). With the heat loss through the heat source pressure vessel known, the heat available to the engine can be calculated from Equation (3.85).

$$Q_e = 250 n_r - Q_{hs} \tag{3.87}$$

The Stirling engine output power is then calculated from this available heat and the engine's efficiency (η_e) as given in Equation (3.88).

$$P_e = \eta_e Q_e \tag{3.88}$$

The engine efficiency is based on the hot end engine temperature and the rejection temperature as given by Equation (3.89). This equation was derived from data on the operation of the Stirling engine over a range of hot end temperatures (Ref. 19).

$$\eta_e = -0.223 + 5.933 \times 10^{-4}\left(T_h - T_r\right) - 3.10 \times 10^{-7}\left(T_h - T_r\right)^2 \tag{3.89}$$

4.0 Analysis Results

The analysis described in Section 3.0 was used to evaluate the airship configuration and flight requirements to determine the size, mass and power to operate near the surface of Venus. An initial sizing was performed to provide a baseline design utilizing 10 GPHS blocks as the heat source that can fly faster than the wind speed near the surface and provide sufficient cooling and power to maintain and operate the payload and electronics. From this design various trades were performed to determine what effect they had on the airship sizing and overall feasibility. These tradeoffs included:

- The flight altitude
- The internal operating temperature of the payload enclosure

4.1 Baseline Airship Design

The goal of the baseline airship design was to provide an airship configuration that could operate near the surface of Venus utilizing 10 GPHS blocks as the power and cooling system heat source. The number of GPHS blocks set the available thermal power at 2500 W, which drove all aspects of the design. The baseline airship configuration is shown in Figure 4.1. This figure represents a proportionally to scale illustration of the airship.

The lifting gas envelope for the airship has an ellipsoidal shape with four control surfaces, fins, symmetrically positioned at the rear of the envelope. Hydrogen is utilized as the lifting gas for the envelope. The two pressure vessels, one for the payload and electronics and the other for the heat source, are positioned one atop the other directly below the envelope. The heat exchanger for the engine sits atop the heat exchanger pressure vessel. The electric motor and propeller is mounted off of the heat source pressure vessel. The electric motor is positioned at the center of mass of the airship. The pressure vessels are attached to the envelope with four struts.

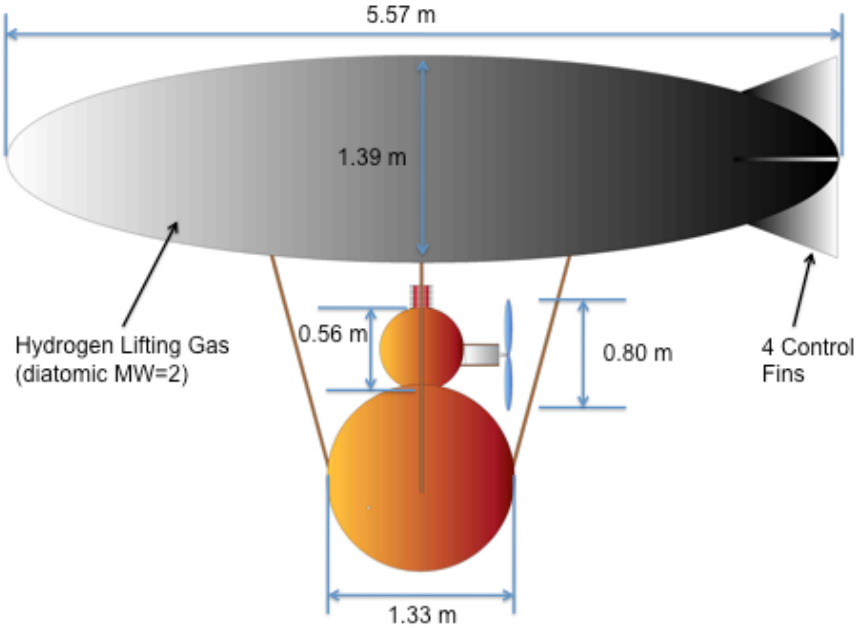

Figure 4.1.—Baseline airship design dimensions.

The main geometry, characteristics and flight specifications for the airship are listed in Table 4.1 and the mass and power breakdowns are given in Table 4.2 and Table 4.3, respectively. The airship was sized so that the available lift and power were equal to or slightly greater than the required lift and power. No additional margin was used in the sizing since power and mass margin was used for sizing of the individual components, as discussed in Section 3.0. The lifting force available for this design point is 3349 N, which corresponds to 375 kg of mass. The total estimated mass of the airship is 374.4 kg, just under the available lift. Similarly the total available power generation capability is 582.5 W, 3.2 W above the required power of 579.3.

TABLE 4.1.—BASELINE AIRSHIP PHYSICAL CHARACTERISTICS

Item	Value
Airship General Specifications	
Airship Fineness Ratio (length to max diameter)	4
Flight altitude	50 m
Flight Velocity (0.5 m/s faster than the max wind speed)	1.39 m/s
Lifting Gas	DiAtomic Hydrogen MW=2
Airship Envelope Length	5.57 m
Airship Envelope Maximum Diameter	1.39 m
Airship Envelope Volume	5.66 m^3
Total Lifting Force (mass)	3349 N (375 kg)
Number of Control Fins	4
Tail Fin Area (per fin)	0.198 m^2
Envelope Material	Metalized Foil 0.25 kg/m^2
Support Strut Material	Carbon-Carbon Composite
Propulsion System	
Propeller Diameter	0.81 m
Propeller Advance Ratio	0.18
Thrust Coefficient	0.01
Power Coefficient	0.003
Propeller Tip Mach Number	0.06
Propeller Efficiency	0.66
Total Driveline Efficiency	0.51
GPHS Block Enclosure and Heat Exchanger	
Heat Source Sphere Outside Diameter	0.56 m
Heat Source Sphere Inside Diameter	0.35 m
Structure:	
Inner Wall	Stainless Steel 1 mm thick
Insulation	Aerogel 10 cm thick
Outer Wall	Carbon/Carbon Composite 4.9 mm thick
Heat Exchanger:	
Number of Cooling Fins	8
Housing Diameter	10 cm
Fin Length	1.5 cm
Fin Thickness	2 m
Electronics/Payload Enclosure	
Electronics Sphere Outside Diameter	1.33 m
Electronics Sphere Inside Diameter	0.90 m
Structure:	
Inner Wall	Aluminum 1 mm thick
Inner Insulation	Aerogel 10.1 cm thick
Middle Wall	Thermo Pyrolytic Graphite 1 mm thick
Outer Insulation	Aerogel 10.1 cm thick
Outer Wall	Carbon/Carbon Composite 1.2 cm thick
Number of wire passthroughs	10
Number of viewports	1

TABLE 4.2.—BASELINE AIRSHIP MASS BREAKDOWN

Item	Mass, kg
Structure (includes envelope, fins and structural support)	98.8
Electric Motor	0.5
Gearbox	0.5
Motor Controller	0.1
Motor Power Conditioning	0.2
Propeller	0.3
Stirling Engine	12.5
Coupling	0.625
Cooler and Alternator	11.38
Flight Control Computer and Electronics	3.8
Communications Equipment	4.6
Sensors and Data Acquisition	3.5
Payload	25
Electronics Pressure Vessel (Includes pressure vessel inner and outer walls, insulation and internal structure)	154.5
GPHS Blocks	14.4
GPHS Block Enclosure (includes inner and outer wall and insulation)	12.6
GPHS Block internal support structure and attachment	12
Cooling Fin	0.19
Struts	2.4
Lifting Gas	16.6
Total Mass	374.4

The drag of the airship is a factor in determining the required airship propulsion power. The drag breakdown for the airship is given in Table 4.3.

TABLE 4.3.—AIRSHIP DRAG BREAKDOWN

Item	Drag, N
GPHS Block Pressure Vessel	1.76
Electronics and Payload Enclosure	10.89
Airship Lifting Gas Envelope	5.30
Heat Exchanger	0.72
Airship Tail	0.89
Support Struts	5.20
Total Drag	24.76

TABLE 4.4.—BASELINE AIRSHIP POWER PRODUCTION AND CONSUMPTION

Variable	Value
Power Production Related Variables	
Total Thermal Power	2500 W
Stirling Engine Hot End Temperature	1473 K
Stirling Engine Cold End Temperature	787.8 K
Stirling Engine Conversion Efficiency	23.9 %
Stirling Engine Output Power	582.5 W
Power Consumption Related Variables	
Electronics Pressure Vessel Internal Temperature	320 K
Heat Loss Through the GPHS Block Enclosure Insulation	62 W
Stirling Cooler Efficiency	44%
Heat Leak Through the Electronics Enclosure Insulation	120.7 W
Heat Leak Through the Passthroughs and View Port	12.85 W
Total Cooling Power Required	390 W
Propulsion System Power Required	67.57 W
Communications, Control and Payload Power	57 W
Total Power Required	579.26 W

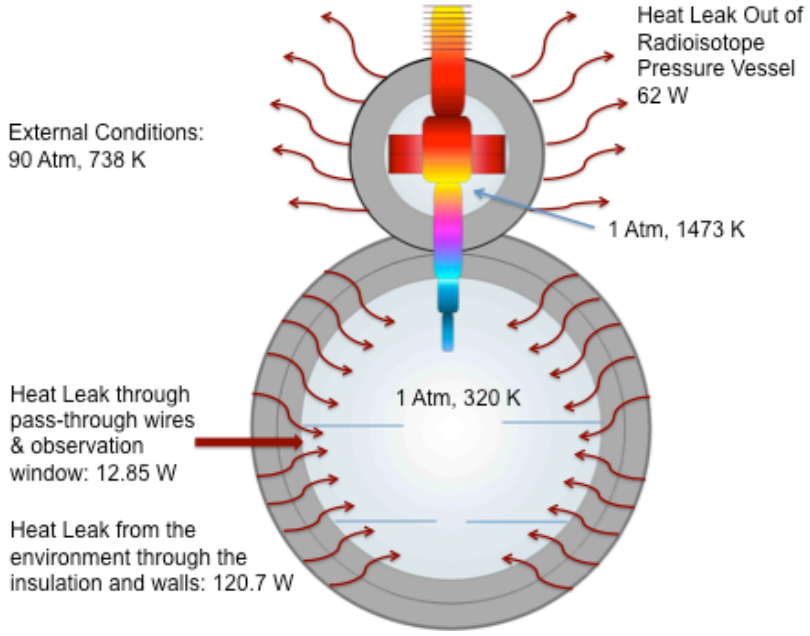

Figure 4.2.—Heat flow into and out of the pressure vessels.

The heat flow from the electronics and heat source pressure vessels is illustrated in Figure 4.2. The values of the parameters, such as the convective heat transfer coefficient, Reynolds number and Nusselt Number, used to determine the heat transfer to and from the pressure vessels and cooling fins is given in Table 4.5.

TABLE 4.5.—CHARACTERISTIC FLOW AND HEAT TRANSFER VALUES FOR THE ENCLOSURES AND HEAT EXCHANGER

Value	Payload/Electronics Enclosure	GPHS Block Enclosure	Engine Waste Heat Cooling Radiator
Nusselt Number	3610 Exterior 78.5 Interior	1674 Exterior 4.1 Interior	113
Reynolds Number	3.4×10^{6} Exterior	1.4×10^{6} Exterior	5.9×10^{4} Fins 2.5×10^{5} Housing
Prandtl Number	0.71 Exterior 0.75 Interior	0.71 Exterior 0.53 Interior	0.71
Raleigh Number	1.6×10^{9} Interior	1.49×10^{5} Interior	N/A
Convective Heat Transfer Coefficient, W/m^2K	159.5 Exterior 1.61 Interior	175.2 Exterior 1.19 Interior	284.7
Insulation thickness	10 cm	2 Layers 10.1 cm each	N/A
Insulation Thermal Conductivity, W/mK	1.7×10^{-2}	1.7×10^{-2}	N/A

4.2 Variation in the Internal Operating Temperature of the Payload Enclosure

One of the main requirements that drive the airship design is the temperature within the electronics and payload enclosure. For the base case this temperature was set at 320 K. To achieve this temperature a Stirling cooler is used, driven by the Stirling engine. This temperature difference, between the interior and the surrounding, plays a large role in the power required as well as the size of the enclosure. The cooling power is dependent on this temperature difference and the subsequent heat leak in from the surroundings. The heat leak is directly related to the amount of insulation within the pressure vessel. For a given interior diameter, the amount of insulation determines the exterior diameter, which in turn affects its mass and drag, the larger the enclosure outside diameter the greater, its mass and drag.

One means of reducing the airship size and power consumption is to increase the temperature within the electronics/payload enclosure. To determine what effect changing the internal temperature has on the total airship cases were run varying the internal temperature. For the first case the baseline geometry (interior diameter and insulation thickness) was maintained and the interior temperature of the enclosure was increased from 320 K to the ambient temperature of 737 K. The required cooling power was determined over this interior temperature range, as shown in Figure 4.3. This figure shows that the cooling power decreases linearly from just above 400 to 91 W at ambient temperature. The 91 W of cooling power was still required at ambient temperature because the waste heat from the electronics and payload must still be removed from within the enclosure.

For the next case the effect of internal temperature on the available internal volume was examined. Instead of reducing cooling power, increasing the interior temperature could be used as a way of providing more interior volume by reducing the insulation thickness while maintaining a constant cooling power. Figure 4.4 show the increase in interior diameter and the corresponding interior volume with increasing internal temperature. Holding the cooling power constant at the baseline level and reducing the insulation thickness achieved this while maintaining the pressure vessel baseline exterior diameter of 1.33 m. As would be expected the internal volume increases from just under 0.4 m^3 at an internal temperature of 320 K to 1.1 m^3 at the atmospheric temperature of 737 K providing a 275 percent increase in volume.

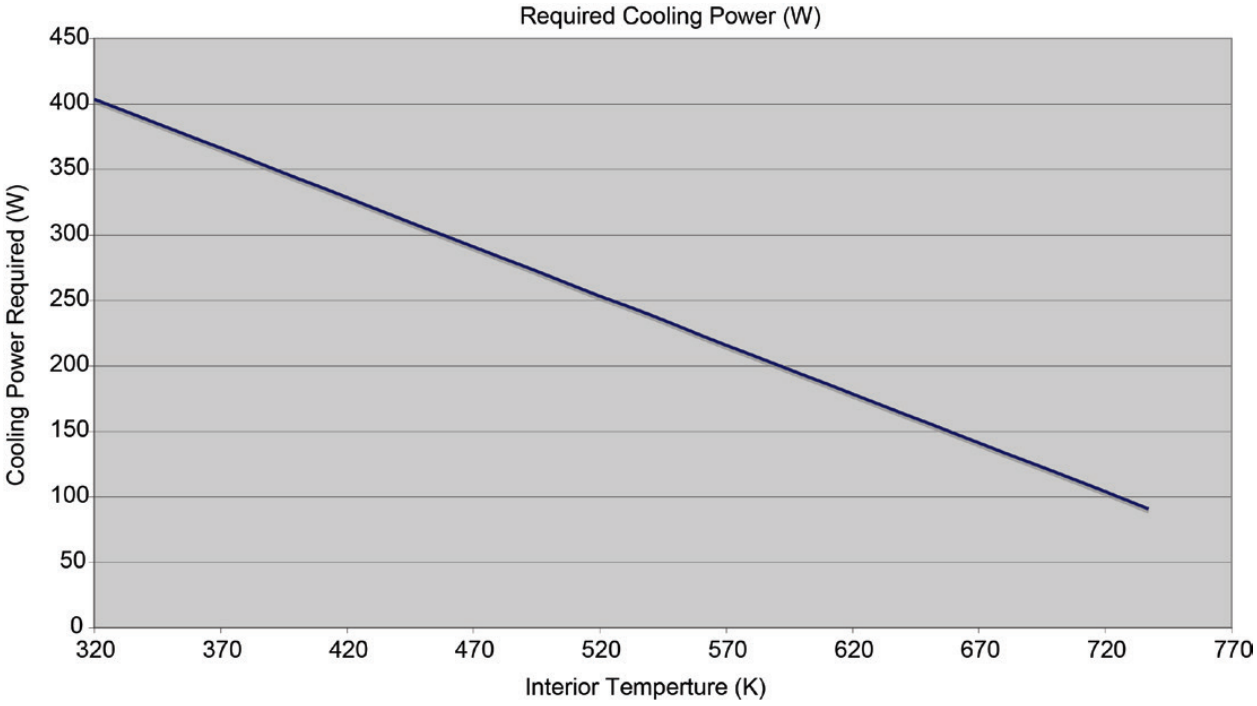

Figure 4.3.—Required cooling power for increasing interior temperature.

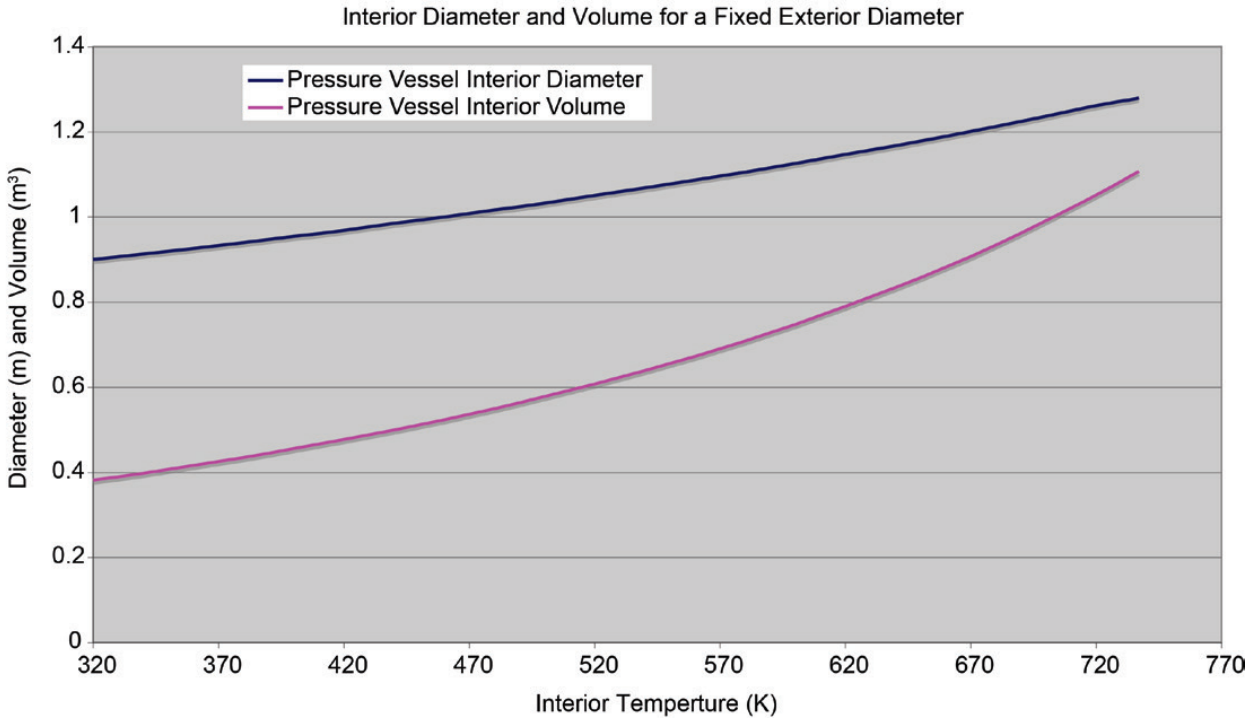

Figure 4.4.—Change in payload enclosure interior diameter and volume with increasing internal temperature.

Another way to evaluate the effect of reducing the required insulation thickness is to maintain a fixed interior volume and decrease the outside diameter of the enclosure. Although with this approach there is no increase in interior volume there is a decrease in the enclosure mass as well as its drag which both factor into the required airship size. This change in exterior diameter as well as the available excess power is shown in Figure 4.5. As the interior temperature was increased, the insulation thickness was reduced so that the cooling power remained the same. Therefore, as shown in the figure, over most of the interior temperature range there is no excess power available. However once the interior temperature gets near 700 K excess power becomes available because there is no more insulation on the interior of the enclosure. Therefore, at this temperature and above the exterior diameter is constant. The wall material does provide some thermal resistance and structurally it must remain at its initial thickness due to the pressure difference between the interior and exterior of the enclosure, 1 and 90 atm, respectively. So with the fixed exterior diameter and an increase in the internal temperature (beyond 700 K), the cooling power therefore decreases providing excess power at this internal temperature and above.

Reducing the payload enclosure diameter has an effect on the overall airship sizing by decreasing its drag and mass. This affect is shown Figure 4.6 where the airship mass decreases from 373 to 243 kg, a reduction of 35 percent, and the length decreases from 5.70 to 4.94 m a reduction of 13 percent for a corresponding temperature increase from 320 K to the atmospheric temperature of 737K.

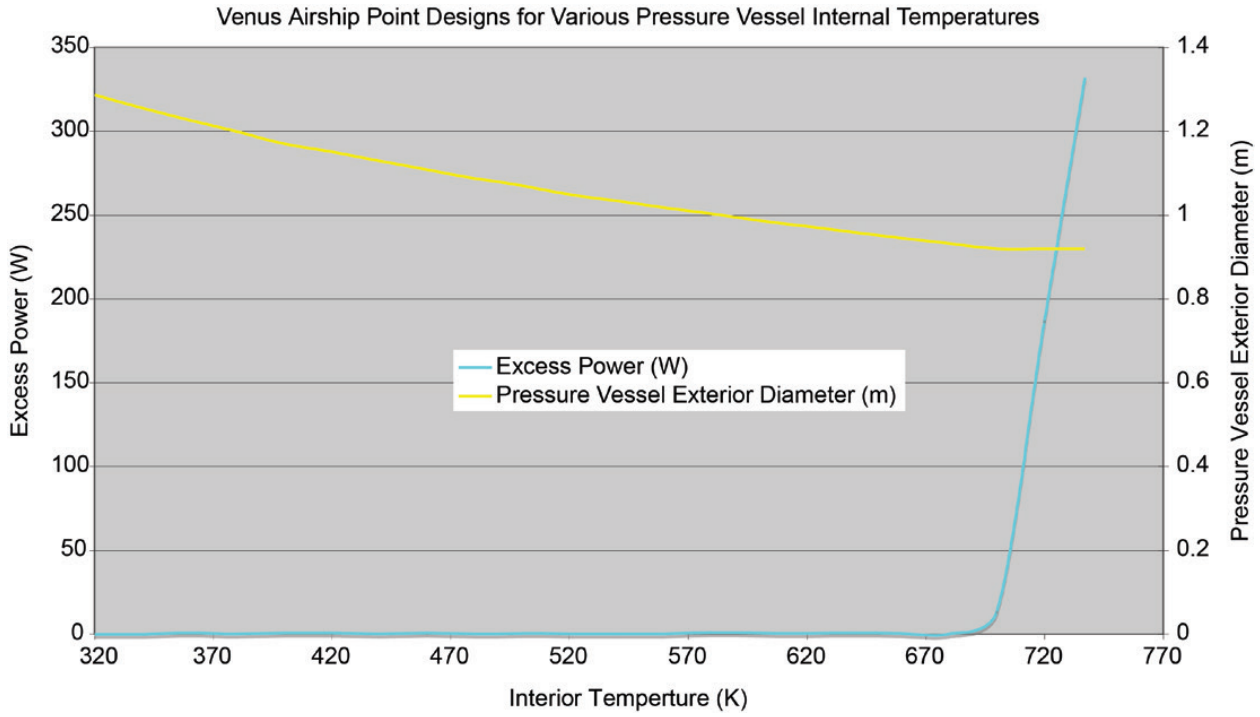

Figure 4.5.—Change in payload enclosure exterior diameter and available excess power with increasing internal temperature.

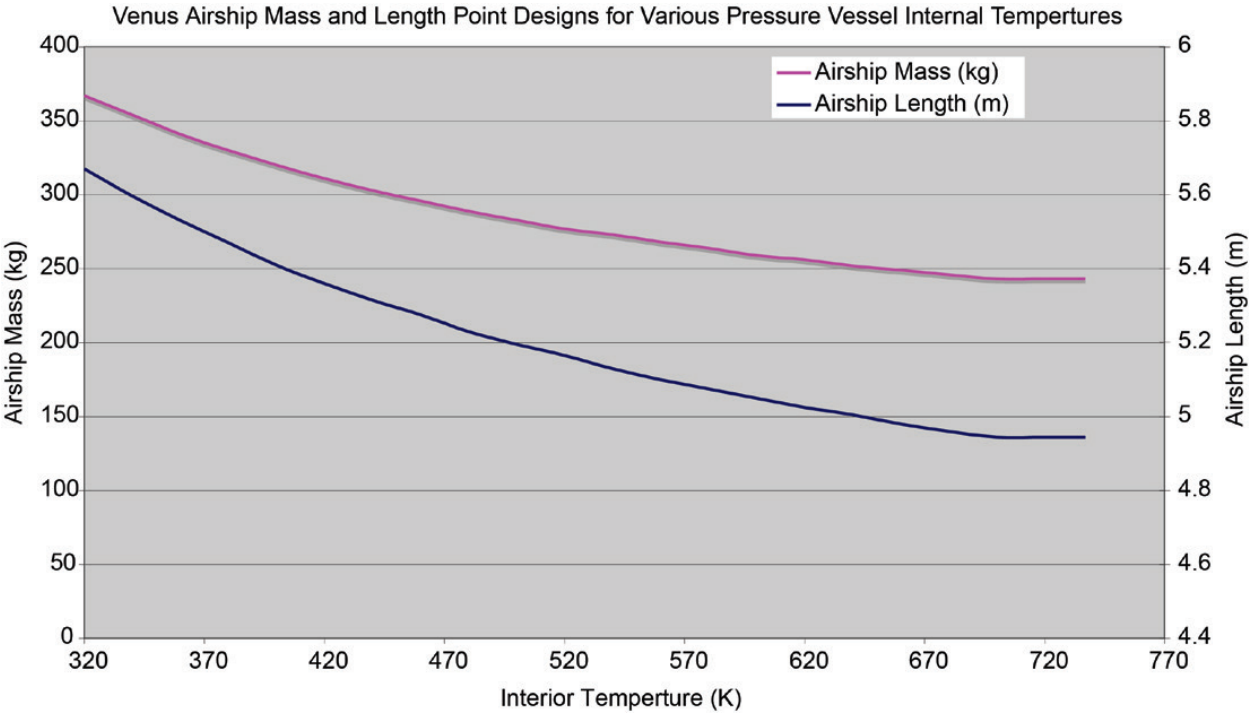

Figure 4.6.—Change in airship total mass and length with increasing enclosure internal temperature.

The temperature evaluation to this point has involved an enclosure designed as a pressure vessel designed to maintain 1 bar of internal pressure. However, if the interior is at atmospheric temperature there is no need for internal insulation and therefore no need to maintain the 1 bar internal pressure. Therefore, operating the enclosure interior at atmosphere temperature and pressure would have the greatest effect on reducing the airship's size, mass and power requirement as shown in Table 4.6. These results show that there is a significant drop in the airship's mass (52.7 percent), required power (60.2 percent) and length (20.1 percent) between the baseline case and operating at atmospheric conditions. This difference is also illustrated in Figure 4.7 and Figure 4.8 for the total vehicle and payload enclosure respectively.

TABLE 4.6.—COMPARISON BETWEEN THE BASELINE AIRSHIP CHARACTERISTICS AND THOSE WITH THE PAYLOAD ENCLOSURE OPERATING AT ATMOSPHERIC CONDITIONS

Variable	Base Case	Payload Enclosure at Atmospheric Temperature and Pressure
Internal Temperature/Pressure	320 K/1 Bar	737 K/90 Bar
Airship Length	5.57 m	4.45 m
Airship Mass	374.4 kg	177 kg
Number of GPHS Blocks	10	4
GPHS Block Interior Enclosure Diameter	0.35 m	0.245 m
Propulsion Power	67.6 W	45 W
Total Power	579.2 W	230.4 W
Enclosure Outside Diameter	1.33 m	0.904 m

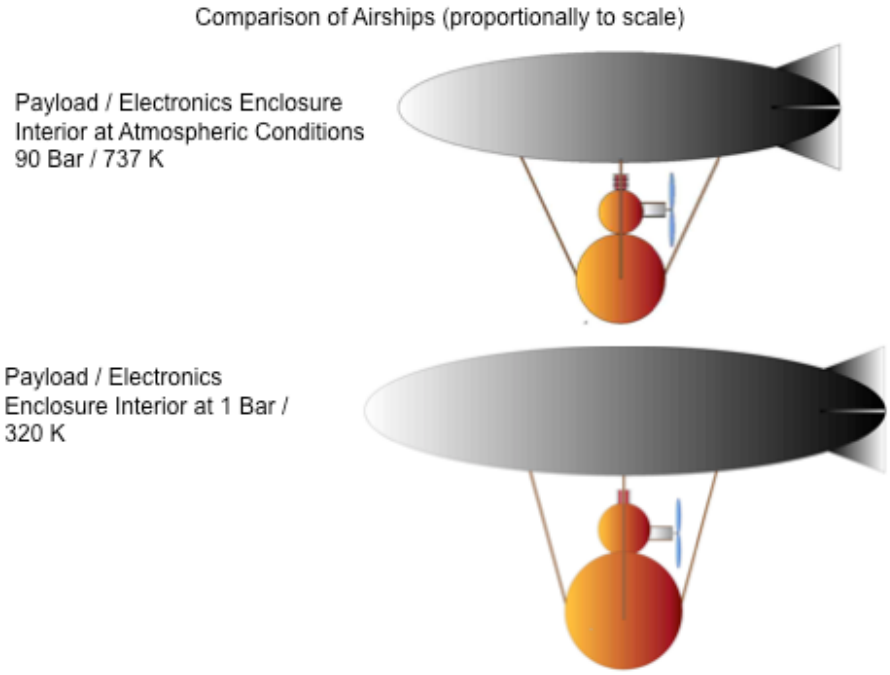

Figure 4.7.—Comparison of the airship size between operating the payload enclosure at the baseline or atmospheric conditions

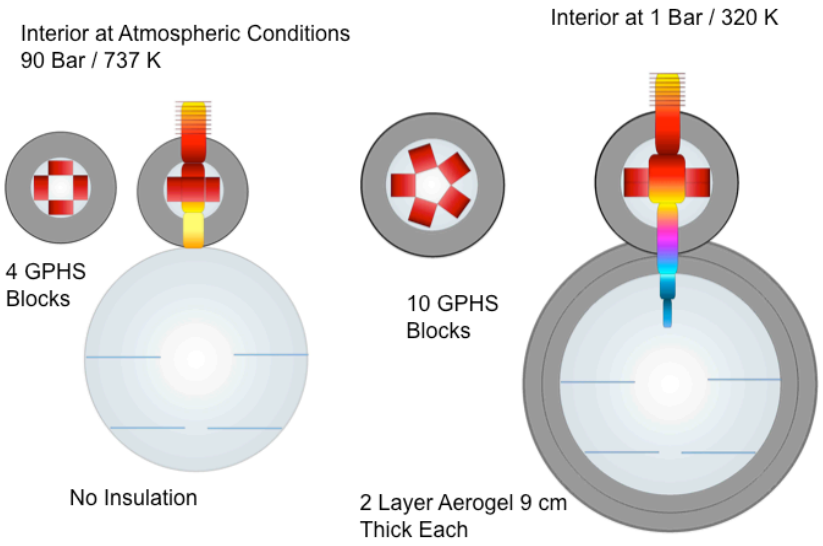

Figure 4.8.—Comparison of the payload and GPHS enclosure geometry between the baseline case and atmospheric conditions.

It should be noted that for the case in which the payload enclosure is operating at atmospheric conditions the GPHS block enclosure must still be kept at 1 atm for the internal insulation to function. The insulation within the heat source enclosure is required to limit the heat loss from the blocks to the surroundings. In this case the payload enclosure utilizes a thin walled vessel. Excess heat generated internal to the vessel is transferred to the exterior through a conductive path to a small radiator on its surface. No active cooling is required. Because there is no cooling requirement the amount of power needed for operating the airship is significantly reduced. Therefore the number of GPHS blocks was reduced from 10 to 4.

As shown in these figures increasing the operating temperature of the interior of the payload enclosure can provide significant benefits in reducing the airship size and mass, with the greatest advantage being when operating at atmospheric conditions. However, being able to construct electronics and other equipment that can survive and function at the temperature and pressure on the surface of Venus will take a considerable development effort over today's capabilities.

4.3 Variation in Flight Altitude

The last evaluation examined the operation of the airship at different altitudes. The airship was sized for flight at altitudes above the baseline case. The airship length was varied from the baseline length in order to provide sufficient lift at the higher altitudes. By changing altitude the environmental conditions, such as the ambient temperature, atmospheric density and wind velocity, changed. The required airship length and corresponding total mass is shown in Figure 4.9 for an altitude range of 50 m (the baseline flight altitude) up to 5.5 km. All aspects of the airship, except the length, remained at the baseline design values.

Figure 4.9 shows that there is a fairly linear increase in airship length and mass with increasing flight altitude. This result would be expected since as the altitude increases the atmospheric density decreases fairly linearly at the lower altitudes, as shown in Figure 2.3. Therefore the lifting force decreases requiring increased lifting gas volume.

Because the baseline airship configuration was used over the altitude range instead of optimizing the configuration, excess power was available over most of the altitude range. The airship's required power and corresponding excess power is shown in Figure 4.10. The reduction in required power, as seen in this figure, as the altitude increased from the baseline altitude was due to the lower drag on the airship as well as the reduction in required cooling power due to the decrease in atmospheric temperature. The minimum required power, of around 420 W, occurs from approximately 2 to 4 km in altitude.

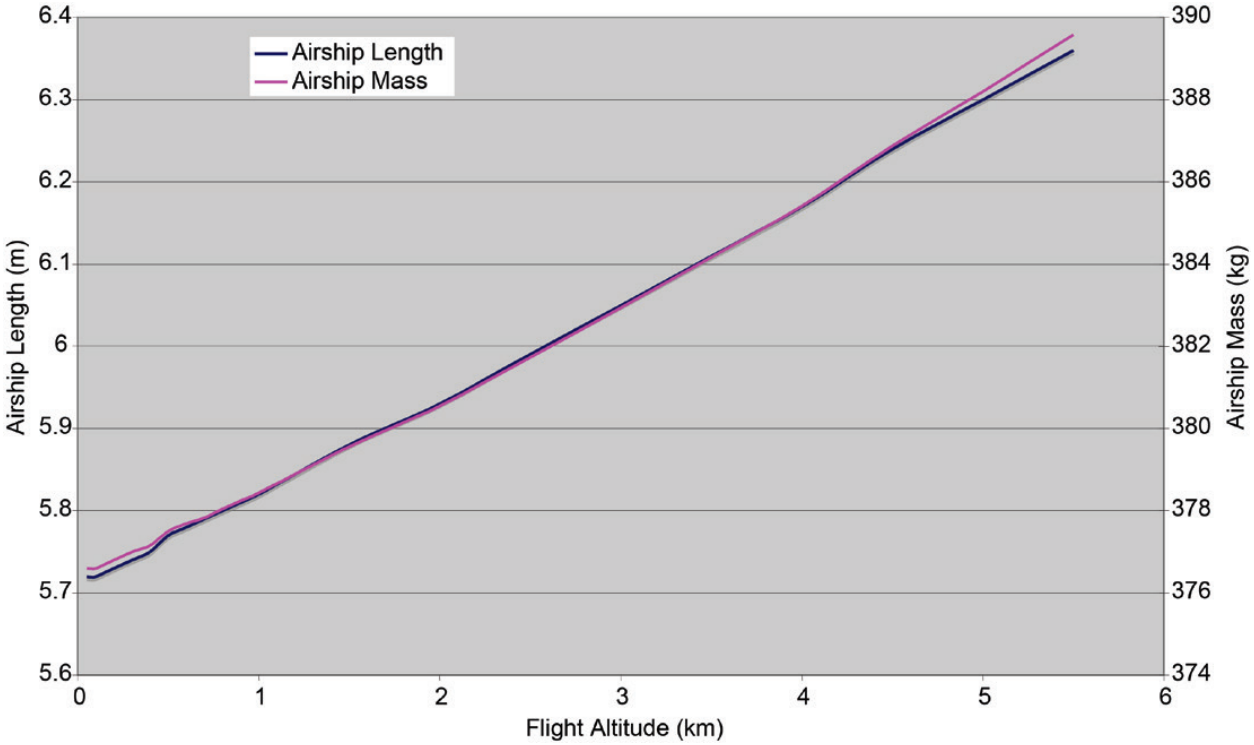

Figure 4.9.—Baseline airship length and mass over a range of flight altitudes.

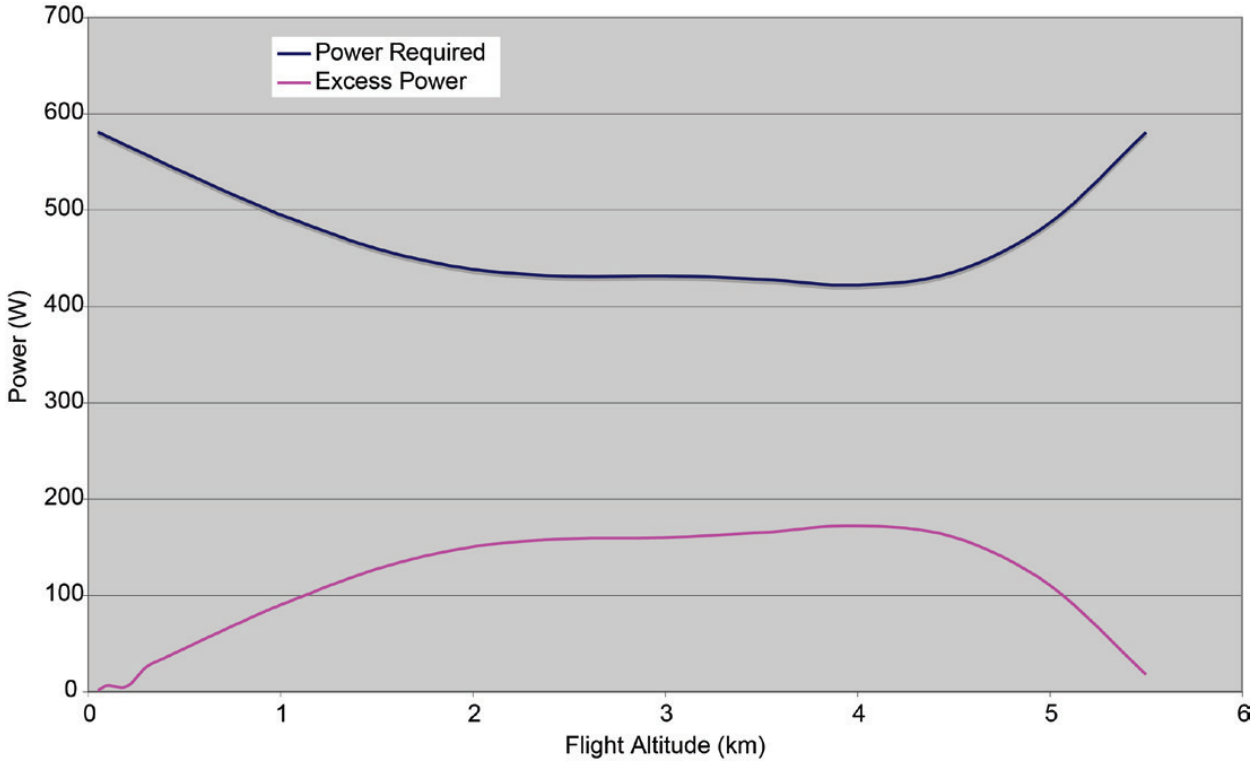

Figure 4.10.—Baseline airship required and excess power over a range of flight altitudes.

This flight altitude range is optimal for minimizing the airship power requirements. Above this range, as can be seen on Figure 4.10, the required power begins to increase sharply to a flight altitude of 5.5 km. Beyond 5.5 km altitude there were no solutions for the baseline airship configuration. The 6.36 m long airship capable of flight at 5.5 km would also be capable of flight down to the baseline airship altitude of 50 m. To achieve this its velocity beyond the wind speed would need to be reduced slightly to 0.49 m/s faster than the winds as it gets closer to the surface.

This altitude analysis shows that an airship 12.4 percent longer (6.36 m versus the baseline airship length of 5.57 m) and 4 percent heaver (387 kg versus the baseline mass of 374.4 kg) can provide a large increase in operational altitude range. Also these results indicate a means of providing additional power to other systems during mission operations. For example if additional power is needed for short periods of time for communications or data processing then, based on these results, the airship could move to an altitude that requires less propulsion and cooling power freeing up power for these other systems.

Another approach, based on these results, would be to design and operate the airship within the minimum power altitude range (2 to 4 km). With the baseline case configuration, an airship designed to operate within this altitude range would require eight GPHS blocks instead of 10.

5.0 Evaluation of Alternate Buoyancy Methods

The analysis, described in Section 3.0, utilizes a lifting gas, at atmospheric conditions, as the means of producing lift for the airship. There are however, other options that can be considered as a means of producing or enhancing lift. These options include:

- A low pressure or vacuum enclosure (similar to a submarine)
- Heated atmospheric gas
- Heated lifting gas

The first of these options would produce lift because the gas density within the lifting gas chamber or envelope would be at a lower density than the atmosphere. The difference in density between the gas within the envelope and the atmosphere would produce lift (L_{pe}), as given by Equation (5.1).

$$L = V_a\left(\rho_a - \frac{P_i}{R_a T_a}\right)g \tag{5.1}$$

To minimize the mass of the chamber used to hold the lower pressure gas, a spherical chamber is needed. This chamber design is similar to that of the payload pressure vessel used in the baseline airship design. The wall thickness of the envelope will need to be strong enough to resist the pressure difference between the interior and exterior pressure. Equation (3.39) can be used to determine the wall thickness needed for the envelope based on this pressure difference. From this wall thickness the mass of the envelope can be determined. This mass along with the corresponding lift generation (in kg) for a 1.25 m diameter sphere is plotted in Figure 5.1. With the atmospheric pressure at 90 bar, internal pressures (P_i) from 60 to 1 bar were examined. From this figure it can be seen that the lift generated is less than the mass of the enclosure itself over this range of internal pressures.

The analysis was also performed with evacuated spheres with diameters between 0.5 and 2.5 m. The results from this analysis are shown in Figure 5.2. From this figure it can be seen that the lift (in kg) was less than the pressure vessel mass over the range of sphere diameters examined (0.5 to 2.5 m). Based on the results shown in these figures it is evident that an evacuated envelope cannot be utilized as the sole means of generating lift on Venus. The weight of the pressure vessel needed to withstand the pressure difference will be larger than the lift generated by the low-pressure volume within it.

The next alternate lift generating approach is to utilize the buoyancy generated by heating the atmospheric gas to a specified temperature. This buoyancy is due to the difference in density between the

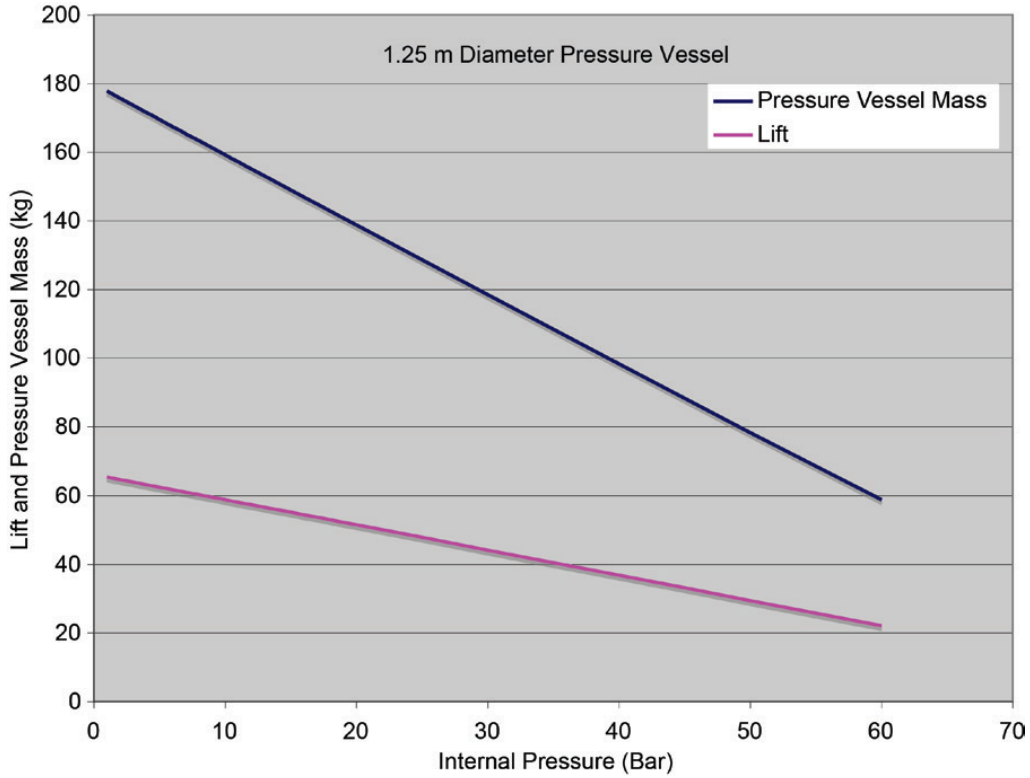

Figure 5.1.—Comparison of mass and lift generation from an evacuated 1.25 m diameter sphere.

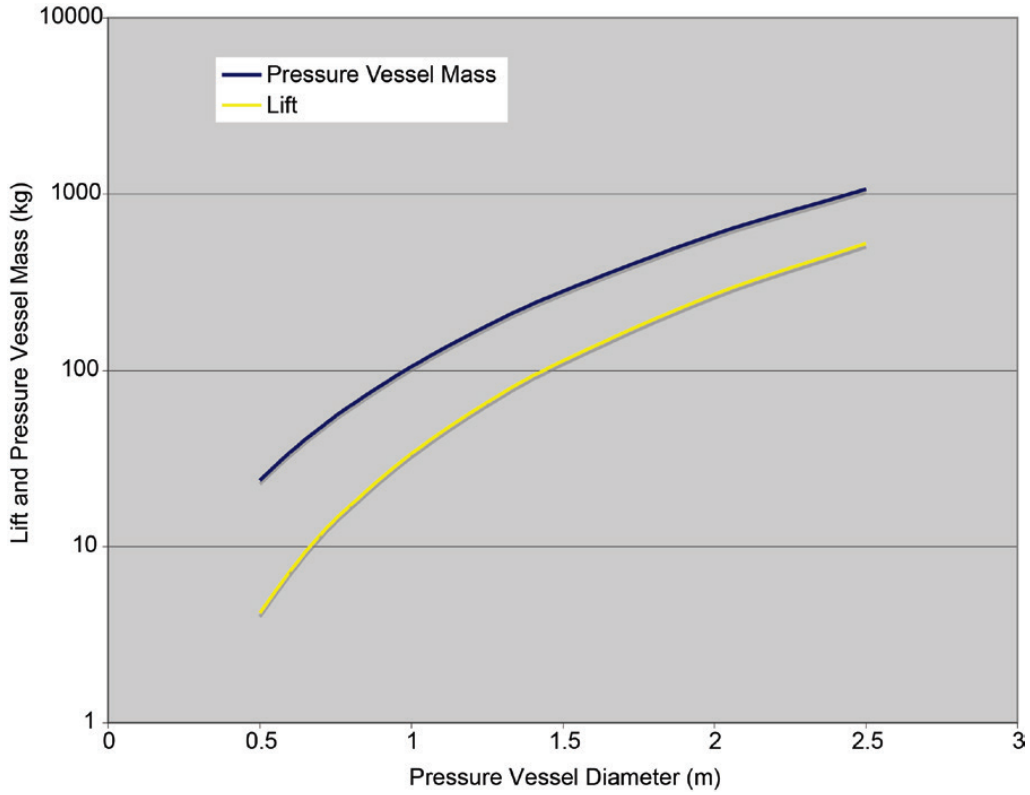

Figure 5.2.—Comparison of mass and lift generation from an evacuated sphere over a range of pressure vessel diameters.

heated atmospheric gas and the atmosphere. Since the atmosphere is comprised mainly of carbon dioxide it was assumed that it would follow the ideal gas equation. Based on this the density of the heated gas within the envelope (ρ_g) is given by Equation (5.2).

$$\rho_g = \frac{P_a}{R_a T_g} \tag{5.2}$$

The waste heat from the Stirling engine will be utilized to heat the atmospheric gas within the envelope. This will cause the engine heat rejection temperature to increase and correspondingly reduce the efficiency of the engine. As an initial evaluation the baseline airship size was used and heated atmospheric gas was used with the baseline envelope volume to generate lift. The temperature of the gas within the envelope was raised from atmospheric to just under the hot end temperature of the engine (1473 K). The lift generated over this temperature range is shown in Figure 5.3. From this figure it can be seen that the lift generated is not sufficient to meet the required lift for the airship. Also, as the temperature difference increases the engine efficiency drops off significantly to a few percent at the largest temperature difference between the lifting gas and the environment.

This analysis indicates that atmospheric heating alone is not sufficient to provide enough lift to meet the mission requirements. Beyond this initial analysis a number of additional factors would also have to be incorporated to fully evaluate this concept. These include:

- The addition of insulation on the gas envelope and the corresponding heat loss from the lifting gas to the environment.
- The effect of the reduction in the engine efficiency on the available power.
- The increase in vehicle drag and propulsion power requirement due to increasing the envelope volume.

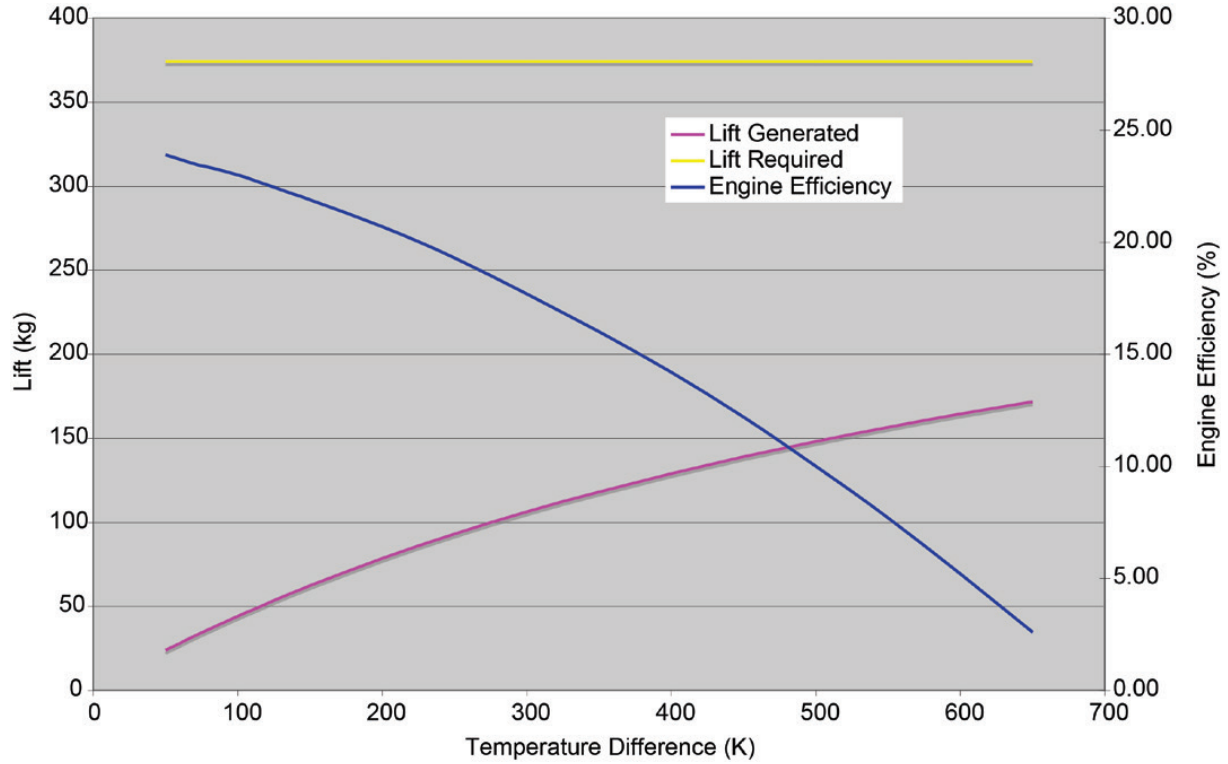

Figure 5.3.—Heated atmosphere gas lift, baseline airship required lift and the corresponding Stirling engine efficiency.

All of these factors would provide a negative impact on the airship sizing. Further analysis could be performed to look at airships with larger envelope sizes or smaller payload capacity, however, based on these results and the additional factors that would have to be included to accurately evaluate this method for generating lift, it was considered to not be feasible within this environment.

Augmenting the lifting gas by heating it was the last alternative method considered for generating lift. In this case the waste heat from the engine was used to heat the hydrogen lifting gas and decrease its density thereby providing additional lift. As with the heated atmosphere case using the waste heat from the engine to heat the lifting gas will increase the engine waste heat rejection temperature and will therefore decrease the efficiency of the engine. This analysis is based on a 50 K temperature difference between the engine rejection temperature and the lifting gas (sink) temperature. This is the same temperature difference that was used with the baseline design. The engine efficiency and corresponding output power for a system with 10 GPHS blocks as the heat source is shown in Figure 5.4. The engine efficiency decreases from 23.9 percent at the baseline case conditions, to 21.9 percent with a 100 K difference between the lifting gas temperature and the atmosphere. This decrease is fairly liner. It should be noted that the fluctuation in the efficiency curve shown in Figure 5.4 is due to round-off error. The corresponding output power drops off proportionally from 583 to 534 W.

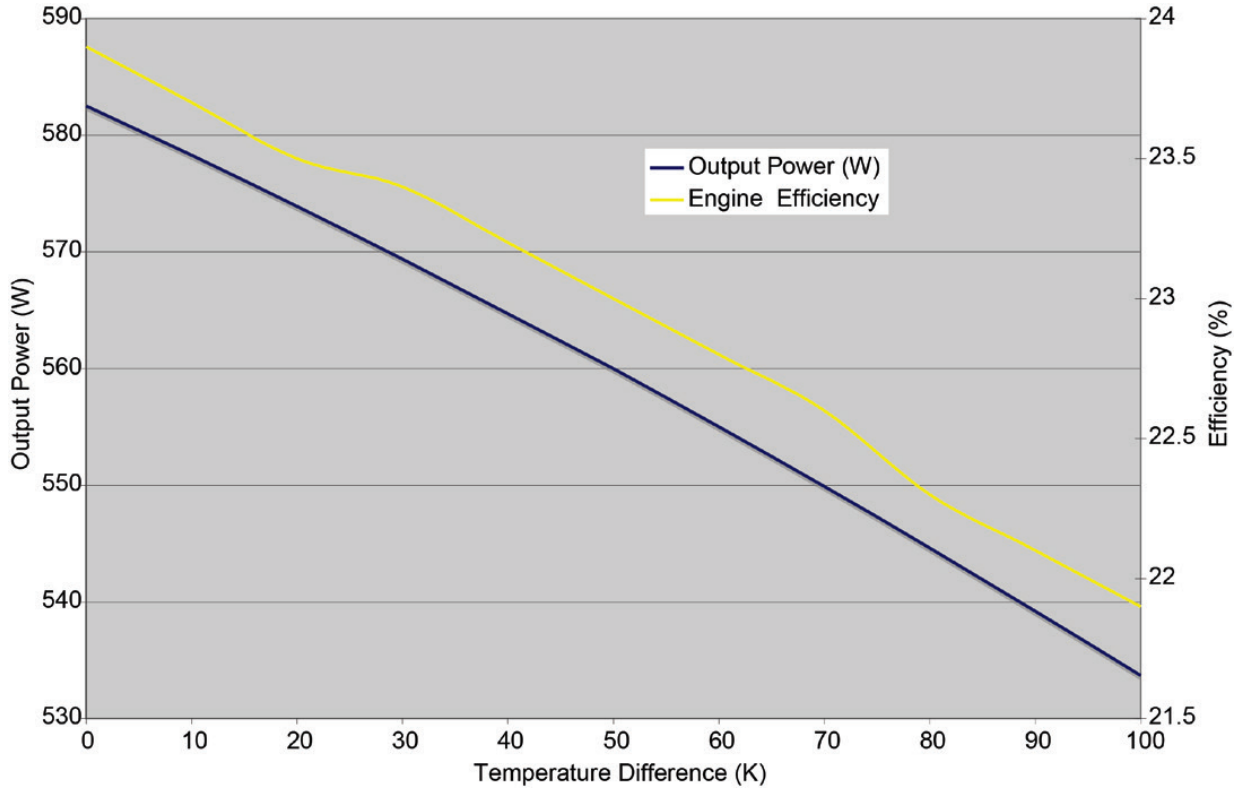

Figure 5.4.—Stirling engine efficiency and output power as a function of the temperature difference between the lifting gas (sink temperature) and the atmosphere temperature.

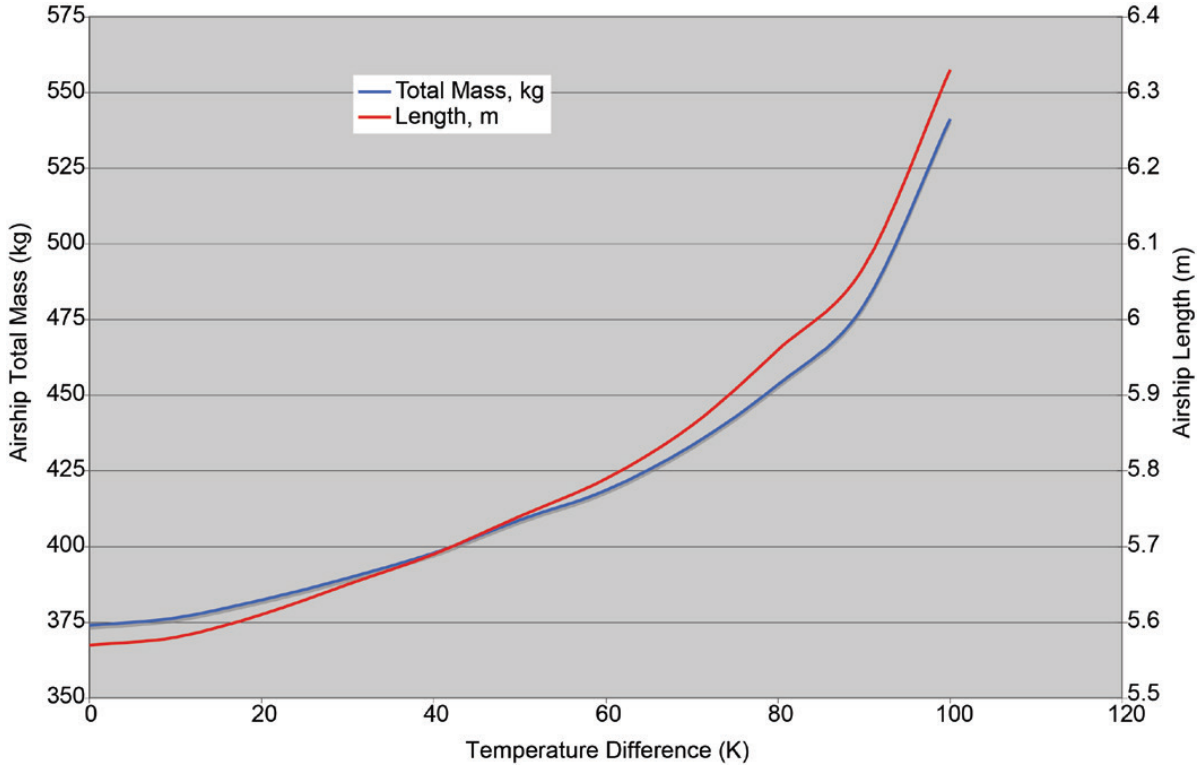

Figure 5.5.—Required airship mass and length as a function of the temperature difference between the lifting gas (sink temperature) and the atmosphere temperature.

Although heating the lifting gas generates additional lift, the reduction in engine efficiency and subsequent available output power has a significant effect on the baseline airship design. Reducing the available power requires additional insulation to be utilized within the payload enclosure to reduce the required cooling power to compensate. This increases the overall diameter of the payload enclosure increasing its mass and drag. The resultant required airship length and corresponding mass for an increase in the lifting gas temperature from atmospheric to 100 K above atmospheric is shown in Figure 5.5.

From this figure it can be seen that the airship size and mass increased exponentially as the temperature of the lifting gas is increased. Therefore there is no benefit gained in the airship sizing by utilizing the waste heat from the engine to heat the lifting gas. The effect of the reduction in engine efficiency overshadows any benefit in additional lift generated by the heated lifting gas.

6.0 Summary

The goal of this analysis was to determine if an airship mission near the surface of Venus is feasible and if that type of mission could be carried out utilizing no more than 10 GPHS blocks as the heat source. Based on the airship analysis and design process outlined in Section 3.0 a baseline airship configuration and size was determined that could meet the mission goals and operate near the Venus surface. This initial analysis indicates that an airship utilizing Hydrogen as the lifting gas is feasible near the surface of Venus. For the baseline design there was sufficient power generated from the 10 GPHS blocks to provide cooling and operate the electronics and propulsion system for the airship.

Off design analysis also provided some insight into some benefits that can be gained by altering the vehicle design and operation. Increasing the interior operating temperature of the electronics/payload enclosure has direct benefits on reducing the airship's size and the overall power requirements. One of the more significant determinations came from evaluating the flight altitude for the airship. From this off-design analysis it was determined that the total required power for the airship is minimized by flying at an altitude

range of between 2 and 4 km and that an airship sized to fly at 5.5 km altitude would be capable of operating over the complete altitude range from near the surface to its design altitude of 5.5 km. This would provide a significant increase in capability over the smaller airship designed specifically for flight near the surface. The flight altitude limit for this airship configuration utilizing 10 GPHS blocks as the main heat source was 5.5 km. For an airship sized to operate above this altitude there was not sufficient power available.

The last evaluation performed examined an alternate means of producing lift for the airship. Of the two alternate methods examined, using a low pressure or evacuated chamber (similar to how a submarine works) and utilizing heated atmospheric gas (similar to a hot-air balloon) neither was capable of providing sufficient lift to raise the airship above the surface. An augmentation of the lifting gas by heating it with waste heat from the engine was also considered. Surprisingly this approach also provided no benefit and in fact increased the airship size over that of the baseline design. The reason this approach failed was that by using the waste heat of the engine to heat the lifting gas the rejection temperature for the engine increased thereby reducing its efficiency. Since engine output power is so critical to the design the reduction in power caused additional insulation to be utilized to maintain the desired internal temperature of the electronics/payload enclosure. This in turn increased its size and mass. Because of this the benefits of increased lift due to the heated lifting gas were overshadowed by the effect of reduced output power from the engine. Thereby providing a net negative benefit.

Since this analysis was setup to determine the initial feasibility of the concept there are a number of areas of the design that warrant further more detailed analysis. These would include the following:

- A detailed analysis of the fluid flow over the pressure vessels and airship envelope. The heat transfer from the insulated pressure vessels is a critical factor in the airship sizing. Any change in this value can have a significant effect on the airship design. The total power required is also affected by the total vehicle drag. Therefore, this analysis would provide a more accurate determination of the heat transfer from the spheres as well as the drag of the airship itself.
- An optimization of the propeller design for operation within the Venus environment. The propeller was a generic design that was not optimized for the Venus environment. Increasing the propeller efficiency could reduce the propulsion system power requirement.
- The operation of the propulsion system drive train (electric motor, gearbox, propeller) within the Venus environment should be evaluated. Because of the harsh environment that they will be exposed to, the physical and material operation of these components could be examined to determine what effect this would have on their performance and operational lifetime.
- A detailed analysis of the internal convection and corresponding heat transfer within the electronics/payload enclosure and the GPHS block enclosure. The heat transfer from the interior gas to the wall of these enclosures has a significant effect on the total heat transfer to and from the surroundings and therefore overall vehicle sizing. Providing a higher fidelity analysis of this heat transfer will correspondingly provide a more accurate determination of the airship sizing. This analysis will also provide a means of evaluating methods for reducing these convective heat transfer coefficients such as putting natural convection barriers along the internal walls.
- The evaluation of a dual stage Stirling cooler. The baseline airship design utilized a single stage Stirling cooler to maintain the internal temperature of the electronics/payload enclosure. A dual stage cooler could also be utilized which could provide increased operational efficiency for the cooler. This increased efficiency would be traded off against removing heat from the first stage over a larger surface area than the single stage cooler.
- A detailed mechanical design for the airship envelope, gas handling and flight control. If it is desired to have the airship change altitude during flight, a ballast system will have to be incorporated so that the airship can change its buoyancy during operation. This ballast system will require mechanical pumps that would have to operate within the Venus environment. Overall a control scheme for the airship could be developed that would include changing altitude as well as direction. Either utilizing the control fins or directing the propeller thrust or both could perform directional changes.

Appendix—List of Symbols

D	Airship Drag
D_e	Gas Envelope Drag
D_h	Heat Source Pressure Vessel Drag
D_{he}	Heat Exchanger Drag
D_p	Payload Pressure Vessel Drag
D_s	Support Strut Drag
D_t	Tail Section Drag
D_{tot}	Total Airship Drag
F_S	Material Yield Factor of Safety
J	Propeller Advance Ratio
L	Airship Lift
M	Mach Number
M_{Wa}	Atmosphere Molecular Weight
M_{Wg}	Lifting Gas Molecular Weight
Nu_{di}	Pressure Vessel Internal Gas Nusselt Number
Nu_{do}	Pressure Vessel External Gas Nusselt Number
Nu_f	Heat Exchanger Nusselt Number
P	Drive Train System Power
P_a	Venus Atmospheric Pressure
P_c	Cooling Power
P_{ce}	Communications Equipment Power
P_e	Stirling Engine Output Power
P_{fc}	Flight Control Computer Power
P_{fs}	Flight Sensor Power
P_i	Pressure Vessel Internal Pressure
P_{pl}	Payload Power
Pr	Prandtl Number
P_r	Total Required Power
Pr_i	Payload Pressure Vessel Internal Prandtl Number
Q_e	Stirling Engine Heat Input
Q_f	Heat Exchanger Fin Heat Transfer
Q_h	Heat Exchanger Housing Heat Transfer
Q_{hs}	Heat Source Pressure Vessel Heat Leak Out
Q_p	Payload Pressure Vessel Heat Leak In
Q_{pw}	Passthrough Wire Heat Leak
Q_{vp}	View Port Heat Leak
Q_w	Stirling Engine Waste Heat
R	Universal Gas Constant
R_a	Atmospheric Gas Constant
Ra_i	Pressure Vessel Internal Gas Rayleigh Number
R_{ci}	Internal Convection Thermal Resistance
R_{co}	External Convection Thermal Resistance

Re_{do} Exterior Pressure Vessel Reynolds Number
Re_f Heat Exchanger Reynolds Number
Re_s Support Strut Reynolds Number
R_f Ratio of Fin Area to Envelope Volume
R_{ii} Inner Insulation Thermal Resistance
R_{io} Outer Insulation Thermal Resistance
R_t Thermal Resistance Term
R_{wi} Inner Wall Thermal Resistance
R_{wm} Middle Wall Thermal Resistance
R_{wo} Outer Wall Thermal Resistance
S_a Airship Envelope Surface Area
S_f Tail Fin Structure Factor
T_a Venus Atmospheric Temperature
T_g Lifting Gas Temperature
T_h Stirling Engine Hot End Temperature
T_i Pressure Vessel Internal Temperature
T_{if} Pressure Vessel Internal Wall Film Temperature
T_r Stirling Engine Heat Rejection Temperature
U Airship Velocity
V_{prop} Propeller Blade Volume
W_{tot} Airship Total Weight
V_a Airship Envelope Volume
a Speed of Sound in the Atmosphere
c_{1c} Cylinder Drag Coefficient Constant 1
c_{1s} Sphere Drag Coefficient Constant 1
c_{2c} Cylinder Drag Coefficient Constant 2
c_{2s} Sphere Drag Coefficient Constant 2
c_{de} Airship Gas Envelope Drag Coefficient
c_{dhe} Heat Exchanger Drag Coefficient
c_{dpv} Pressure Vessel Drag Coefficient
c_{ds} Support Strut Drag Coefficient
c_{oc} Cylinder Drag Coefficient Constant 0
c_{os} Sphere Drag Coefficient Constant 0
c_p Propeller Power Coefficient
c_{pa} Atmosphere Specific Heat
c_{pi} Pressure Vessel Internal Gas Specific Heat
c_t Propeller Thrust Coefficient
d Airship Envelope Maximum Diameter
d_e Heat Rejection Housing Diameter
d_f Heat Rejection Outer Fin Diameter
d_h Heat Exchanger Hydraulic Diameter
d_{prop} Propeller Diameter
d_{pv} Pressure Vessel Diameter
d_s Support Strut Diameter

d_{vp} View Port Diameter
d_w Pass Through Wire Diameter
f Airship Envelope fineness ratio
f_f Cooling Fin Friction Factor
g Venus Gravitational Acceleration
h_f Waste Heat Exchanger Convective Coefficient
h_i Pressure Vessel Internal Convection Coefficient
h_o Pressure Vessel External Convection coefficient
k_a Atmosphere Thermal Conductivity
k_{hi} Heat Source Pressure Vessel Insulation Conductivity
k_{hwi} Heat Source Pressure Vessel Inner Wall Conductivity
k_{hwo} Heat Source Pressure Vessel Outer Wall Conductivity
k_i Pressure Vessel Internal Gas Thermal Conductivity
k_{ii} Inner Insulation Thermal Conductivity
k_{io} Outer Insulation Thermal Conductivity
k_m Material Layer Thermal Conductivity
k_{vp} View Port Material Thermal Conductivity
k_w Pass Through Wire Thermal Conductivity
k_{wi} Inner Wall Thermal Conductivity
k_{wm} Middle Wall Thermal Conductivity
k_{wo} Outer Wall Thermal Conductivity
l Airship Envelope Length
l_e Heat Rejection Housing Length
l_s Support Strut Length
m_{ca} Stirling Engine Cooler and Alternator Mass
m_{ce} Communication Equipment Mass
m_{dt} Drive Train Total Mass
m_{em} Electric Motor Mass
m_f Heat Exchanger Cooling Fin Mass
m_{fc} Flight Control Computer Mass
m_{fi} Fixed Item Mass
m_{fs} Flight Control Computer Mass
m_g Gearbox Mass
m_{hi} Heat Source Pressure Vessel Insulation Mass
m_{hv} Heat Source Pressure Vessel Mass
m_{hwi} Heat Source Pressure Vessel Inner Wall Mass
m_{hwo} Heat Source Pressure Vessel Outer Wall Mass
m_{ii} Payload Pressure Vessel Inner Insulation Mass
m_{io} Payload Pressure Vessel Outer Insulation Mass
m_{lg} Lifting Gas Mass
m_{mc} Motor Controller Mass
m_p Payload Pressure Vessel Mass
m_{pc} Power Conditioning Mass
m_{pi} Payload Pressure Vessel Inner Wall Mass

m_{pl} Payload Mass
m_{pm} Payload Pressure Vessel Middle Wall Mass
m_{po} Payload Pressure Vessel Outer Wall Mass
m_{prop} Propeller Mass
m_{ps} Power System Mass
m_r Total Radioisotope Bock Mass
m_s Airship Structure Mass
m_{se} Stirling Engine Mass
m_{sepc} Stirling Engine Pneumatic Coupling Mass
m_{ss} Support Strut Mass
m_{tot} Total Airship Mass
n_b Number of Propeller Blades
n_{cf} Number of Heat Rejection Cooling Fins
n_f Number of Tail Fins
n_r Number of Radioisotope Blocks
n_s Number of Support Struts
n_{vp} Number of View Ports
n_w Number of Pass-through Wires
r_{hi} Heat Source Pressure Vessel Inner Radius
r_{ho} Heat Source Pressure Vessel Outer Radius
r_i Material Layer Internal Radius
r_o Material Layer Outer Radius
r_{pi} Payload Pressure Vessel Inner Radius
r_{po} Payload Pressure Vessel Outer Radius
t_f Heat Rejection Fin Thickness
t_{hi} Heat Source Pressure Vessel Insulation Thickness
t_{hwi} Heat Source Pressure Vessel Inner Wall Thickness
t_{hwo} Heat Source Pressure Vessel Outer Wall Thickness
t_{ii} Payload Pressure Vessel Inner Insulation Thickness
t_{io} Payload Pressure Vessel Outer Insulation Thickness
t_{pi} Payload Pressure Vessel Inner Wall Thickness
t_{pm} Payload Pressure Vessel Middle Wall Thickness
t_{po} Payload Pressure Vessel Outer Wall Thickness
v_a Venus Atmospheric Wind Velocity
v_b Propeller Blade Internal Void Fraction
z Altitude above the Surface
α_i Pressure Vessel Internal Gas Thermal Diffusivity
ΔT_{wi} Difference Between the Pressure Vessel Wall and Interior Temperature
η_c Cooler Efficiency
η_e Stirling Engine Operating Efficiency
η_{em} Electric Motor Efficiency
η_g Gearbox Efficiency
η_{mc} Motor Controller Efficiency

η_p Propulsion System Efficiency
η_{prop} Propeller Efficiency
μ_a Venus Atmospheric Dynamic Viscosity
μ_i Pressure Vessel Internal Gas Dynamic Viscosity
ν_i Pressure Vessel Internal Gas Kinematic Viscosity
ρ_a Venus Atmospheric Density
ρ_e Envelope Material Aerial Density
ρ_f Cooling Fin Material Density
ρ_g Lifting Gas Density
ρ_i Pressure Vessel Insulation Density
ρ_{hwo} Heat Source Pressure Vessel Outer Wall Material Density
ρ_{hwi} Heat Source Pressure Vessel Inner Wall Material Density
ρ_{prop} Propeller Material Density
ρ_{pi} Payload Pressure Vessel Inner Wall Material Density
ρ_{pm} Payload Pressure Vessel Middle Wall Material Density
ρ_{po} Payload Pressure Vessel Outer Wall Material Density
ρ_s Support Strut Material Density
σ_{ypo} Pressure Vessel Outer Wall Yield Strength

References

1. Loders, K., and Fegley, G. Jr., "Venus," The Planetary Scientist's Handbook, pp. 109-124, Oxford University Press 1998.
2. Mitchell, D.P., Venera 13 Perspective Image Mosaics, http://mentallandscape.com/C_CatalogVenus.htm, June 2011.
3. Colozza, A., "Airships for Planetary Exploration," NASA/CR—2004-213345, November 2004.
4. Saunders, R. S., "Venus," in The New Solar System, 4th Edition, (Beatty, J.K., Petersen, C.C., and Chaikin, A., eds.), Cambridge University Press, 2000.
5. Ekonomov, A., Golovin, Yu., Moroz, V., and Moshkin, B., "19: Solar Scattered Radiation Measurements by Venus Probes," Venus, University of Arizona Press 1983.
6. Jenkins, J.M., Steffes, P.G., Hinson, D.P., Twicken, J.D., and Tyler, G.L., in "Radio Occultation Studies of the Venus Atmosphere with the Magellan Spacecraft," Icarus, Vol. 110, pp. 79-94, 1994.
7. Colozza, A.J., "Solar Powered Flight on Venus," NASA/CR—2004-213052, April 2004.
8. Colozza, A.J., "High Altitude Propeller Design and Analysis Overview," NASA/CR—1998-208520, October 1998.
9. Colozza, A.J., "Initial Feasibility Assessment of a High Altitude Long Endurance Airship," NASA/CR—2003-212724, December 2003.
10. Colozza, A.J., "Comparison of Mars Aircraft Propulsion Systems," NASA CR-2003-212350, May 2003.
11. Incropera, F.P., and DeWitt, D.P., Fundamentals of Heat and Mass Transfer, Third Edition, John Wiley & Sons Publisher, 1990.
12. White, F. M., Fluid Mechanics, McGraw-Hill Publisher, 1979.
13. Khoury, G.A. and Gillett, J.D., editors, Airship Technology, Cambridge Aerospace Series 10, Cambridge University Press, 1999.
14. Achenbach, E., "Experiments of the Flow Past Spheres at Very High Reynolds Numbers," Journal of Fluid Mechanics, Vol. 54, part 3, pp. 565-575, 1972.
15. Wang,Y.Q., Jackson, P.L., and Ackerman, J.D., "Numerical Investigation of Flow over a Sphere using LES and the Spalart-Allmaras Turbulence Model," Journal of Computational Fluid Dynamics, Vol. 15, No. 1, pp. 198-205, April 2006.
16. Achenbach, E., "Total and Local Heat Transfer from a Smooth Circular Cylinder in Cross-Flow at High Reynolds Number," Journal of Heat and Mass Transfer, Vol. 18, pp. 1387-1396, 1975.
17. Churchill, S.W., and Bernstein, M., "A Correlation Equation for Forced Convection from Gases and Liquids to a Circular Cylinder in Cross Flow," Journal of Heat and Mass Transfer, ASME 94, pp. 300-306, 1977.
18. "Space and Defense Power Systems," U.S. Department of Energy, www.ne.doe.gov, October 2011.
19. Dyson, R.W., "Advanced Stirling Duplex: Technology Advancement Project Review," March 2011.

REPORT DOCUMENTATION PAGE			Form Approved OMB No. 0704-0188

1. REPORT DATE *(DD-MM-YYYY)*	2. REPORT TYPE	3. DATES COVERED *(From - To)*
01-08-2012	Final Contractor Report	

4. TITLE AND SUBTITLE
Radioisotope Stirling Engine Powered Airship for Low Altitude Operation on Venus

5a. CONTRACT NUMBER
NNC07E252T-8

5b. GRANT NUMBER

5c. PROGRAM ELEMENT NUMBER

6. AUTHOR(S)
Colozza, Anthony, J.

5d. PROJECT NUMBER

5e. TASK NUMBER

5f. WORK UNIT NUMBER
WBS 138494.04.01.03

7. PERFORMING ORGANIZATION NAME(S) AND ADDRESS(ES)
Qinetiq North America
21000 Brookpark Road
Cleveland, Ohio 44135

8. PERFORMING ORGANIZATION REPORT NUMBER
E-18342

9. SPONSORING/MONITORING AGENCY NAME(S) AND ADDRESS(ES)
National Aeronautics and Space Administration
Washington, DC 20546-0001

10. SPONSORING/MONITOR'S ACRONYM(S)
NASA

11. SPONSORING/MONITORING REPORT NUMBER
NASA/CR-2012-217665

12. DISTRIBUTION/AVAILABILITY STATEMENT
Unclassified-Unlimited
Subject Categories: 01, 05, 06, and 91
Available electronically at http://www.sti.nasa.gov
This publication is available from the NASA Center for AeroSpace Information, 443-757-5802

13. SUPPLEMENTARY NOTES

14. ABSTRACT
The feasibility of a Stirling engine powered airship for the near surface exploration of Venus was evaluated. The heat source for the Stirling engine was limited to 10 general purpose heat source (GPHS) blocks. The baseline airship utilized hydrogen as the lifting gas and the electronics and payload were enclosed in a cooled insulated pressure vessel to maintain the internal temperature at 320 K and 1 Bar pressure. The propulsion system consisted of an electric motor driving a propeller. An analysis was set up to size the airship that could operate near the Venus surface based on the available thermal power. The atmospheric conditions on Venus were modeled and used in the analysis. The analysis was an iterative process between sizing the airship to carry a specified payload and the power required to operate the electronics, payload and cooling system as well as provide power to the propulsion system to overcome the drag on the airship. A baseline configuration was determined that could meet the power requirements and operate near the Venus surface. From this baseline design additional trades were made to see how other factors affected the design such as the internal temperature of the payload chamber and the flight altitude. In addition other lifting methods were evaluated such as an evacuated chamber, heated atmospheric gas and augmented heated lifting gas. However none of these methods proved viable.

15. SUBJECT TERMS
Airships; Radioisotope heat sources; Stirling engines; Venus probes; Planetary aerial vehicles

16. SECURITY CLASSIFICATION OF:			17. LIMITATION OF ABSTRACT	18. NUMBER OF PAGES	19a. NAME OF RESPONSIBLE PERSON
a. REPORT	b. ABSTRACT	c. THIS PAGE			STI Help Desk (email:help@sti.nasa.gov)
U	U	U	UU	58	19b. TELEPHONE NUMBER *(include area code)* 443-757-5802